Spatial and temporal variations of dissolved greenhouse gases (CO_2, CH_4, N_2O) in the Congo River network

Alberto V. Borges[1,*], François Darchambeau[1,**], Thibault Lambert[1,***], Cédric Morana[2], George H. Allen[3], Ernest Tambwe[4], Alfred Toengaho Sembaito[4], Taylor Mambo[4], José Nlandu Wabakhangazi[5], Jean-Pierre Descy[1], Cristian R. Teodoru[2,****], Steven Bouillon[2]

[1] Chemical Oceanography Unit, University of Liège, Liège, Belgium
[2] Department of Earth and Environmental Sciences, KULeuven, Leuven, Belgium
[3] Department of Geography, Texas A&M University, USA
[4] Université de Kisangani, Centre de Surveillance de la Biodiversité, DRC Congo
[5] Congo Atomic Energy Commission, Kinshasa, DRC Congo

[*] alberto.borges@uliege.be
[**] Present address: Direction générale opérationnelle Agriculture, Ressources naturelles et Environnement, Service Publique de Wallonie, Belgium
[***] Present address: University of Lausanne, Institute of Earth Surface Dynamics, Lausanne, Switzerland
[****] Present address: Eidgenössische Technische Hochschule Zürich, Switzerland.

Abstract

We carried out ten field expeditions between 2010 and 2015, in the lowland part of the Congo River network in the eastern part of the basin (Democratic Republic of Congo), to describe the spatial variations of fluvial dissolved carbon dioxide (CO_2), methane (CH_4), and nitrous oxide (N_2O) concentrations. We investigate the possible drivers of the spatial variations of dissolved CO_2, CH_4 and N_2O concentrations by analysing co-variations with several other biogeochemical variables, aquatic metabolic processes (primary production and respiration), catchment characteristics (land cover) and wetland spatial distribution. We test the hypothesis that spatial patterns of CO_2, CH_4 and N_2O are partly due to the connectivity with wetlands, in particular with a giant wetland of flooded forest in the core of the Congo basin, the "Cuvette Centrale Congolaise" (CCC). Two transects of 1,650 km were carried out from the city of Kisangani to the city of Kinshasa, along the longest possible navigable section of the river, and corresponding to 41% of the total length of the mainstem. Additionally, three time series of CH_4 and N_2O were obtained at fixed points in the mainstem of the middle Congo (2013-2018, biweekly sampling), in the mainstem of the lower Kasaï (2015-2017, monthly sampling), and in the mainstem of the middle Oubangui (2010-2012, biweekly sampling). The variations of dissolved N_2O concentrations were modest, with values oscillating around the concentration corresponding to saturation with the atmosphere, with N_2O saturation level (%N_2O, where atmospheric equilibrium corresponds to 100%) ranging between 0% and 561% (average 142%). The relatively narrow range of %N_2O variations was consistent with low NH_4^+ (2.3±1.3 µmol L^{-1}) and NO_3^- (5.6±5.1 µmol L^{-1}) levels in these near pristine rivers and streams with low agriculture pressure on the catchment (croplands correspond to 0.1% of catchment land cover of sampled rivers), dominated by forests (~70% of land cover). The co-variations of %N_2O, NH_4^+, NO_3^-, and dissolved oxygen saturation level (%O_2) indicate N_2O removal by soil or sedimentary denitrification in low O_2, high NH_4^+ and low NO_3^- environments (typically small and organic matter rich streams) and N_2O production by nitrification in high O_2, low NH_4^+ and high NO_3^- (typical of larger rivers that are poor in organic matter). Surface waters were very strongly over-saturated in CO_2 and CH_4 with respect to atmospheric equilibrium, with values of the partial pressure of CO_2 (pCO_2) ranging between 1,087 and 22,899 ppm (equilibrium ~400 ppm), and dissolved CH_4

concentrations ranging between 22 and 71,428 nmol L^{-1} (equilibrium ~2 nmol L^{-1}). Spatial variations were overwhelmingly more important than seasonal variations for pCO_2, CH_4 and $\%N_2O$, and than diurnal (day-night) variations for pCO_2. The wide range of pCO_2 and CH_4 variations was consistent with the equally wide range of $\%O_2$ (0.3-122.8%) and of dissolved organic carbon (DOC) (1.8-67.8 mg L^{-1}), indicative of generation of these two greenhouse gases from intense processing of organic matter either in *terra firme* soils, wetlands or in-stream. However, the emission rate of CO_2 to the atmosphere from riverine surface waters was on average about 10 times higher than the flux of CO_2 produced by aquatic net heterotrophy (as evaluated from measurements of pelagic respiration and primary production). This indicates that the CO_2 emissions from the river network were sustained by lateral inputs of CO_2 (either from *terra firme* or from wetlands). The pCO_2 and CH_4 values decreased and $\%O_2$ increased with increasing Strahler order, showing that stream size explains part of the spatial variability of these quantities. In addition, several lines of evidence indicate that lateral inputs of carbon from wetlands (flooded forest and aquatic macrophytes) were of paramount importance in sustaining high CO_2 and CH_4 concentrations in the Congo river network, as well as driving spatial variations: the rivers draining the CCC were characterized by significantly higher pCO_2 and CH_4 and significantly lower $\%O_2$ and $\%N_2O$ values than those not draining the CCC; pCO_2 and $\%O_2$ values were correlated to the coverage of flooded forest on the catchment. The flux of GHGs between rivers and the atmosphere averaged 2,469 mmol m^{-2} d^{-1} for CO_2 (range 86 and 7,110 mmol m^{-2} d^{-1}), 12,553 µmol m^{-2} d^{-1} for CH_4 (range 65 and 597,260 µmol m^{-2} d^{-1}), 22 µmol m^{-2} d^{-1} for N_2O (range -52 and 319 µmol m^{-2} d^{-1}). The estimate of integrated CO_2 emission from the Congo River network (251±46 TgC (10^{12} gC) yr^{-1}) corresponded to nearly half the CO_2 emissions from tropical oceans globally (565 TgC yr^{-1}) and was nearly two times the CO_2 emissions from the tropical Atlantic Ocean (137 TgC yr^{-1}). Moreover, the integrated CO_2 emission from the Congo River network is more than three times higher than the estimate of terrestrial net ecosystem exchange (NEE) on the whole catchment (77 TgC yr^{-1}). This shows that it is unlikely that the CO_2 emissions from the river network were sustained by the hydrological carbon export from *terra firme* soils (typically very small compared to terrestrial NEE), but most likely, to a large extent, they were sustained by wetlands (with a much higher hydrological connectivity with rivers and streams).

Keywords: Africa; Congo River, carbon dioxide, methane, nitrous oxide, tropical wetlands; tropical rivers

1. Introduction

Emissions to the atmosphere of greenhouse gases (GHGs) such as carbon dioxide (CO_2), methane (CH_4) and nitrous oxide (N_2O) from inland waters (rivers, lakes and reservoirs) might be quantitatively important for global budgets (Seitzinger and Kroeze 1998; Cole et al. 2007; Bastviken et al. 2011). Yet, there are very large uncertainties in the estimates of GHGs emission to the atmosphere from rivers, as reflected in the wide range of reported values, between 0.2 and 1.8 PgC (10^{15} gC) yr^{-1} for CO_2 (Cole et al. 2007; Raymond et al. 2013), 2 and 27 TgCH$_4$ (10^{12} gCH$_4$) yr^{-1} for CH_4 (Bastviken et al. 2011; Stanley et al. 2016), 32 and 2100 GgN$_2$O-N (10^9 gN$_2$O-N) yr^{-1} for N_2O (Kroeze et al. 2010; Hu et al. 2016). This uncertainty is mainly due to the scarcity of data in the tropics that account for the majority of riverine GHG emissions (~80% for CO_2 (Raymond et al. 2013; Borges et al. 2015a,b; Lauerwald et al. 2015), 79% for N_2O (Hu et al. 2016), 70% for CH_4 (Sawakushi et al. 2014)), but also to scaling procedures of varying complexity that use different input data (Raymond et al. 2013; Borges et al. 2015b; Lauerwald et al. 2015), in addition to uncertainty on the estimate of surface area of rivers (Downing et al. 2012; Raymond et al. 2013; Allen and Pavelsky 2018), and the parameterisation of the gas transfer velocity (k) (Raymond et al. 2012; Huotari et al. 20013; Maurice et al. 2017; Kokic et al. 2018; McDowell and Johnson 2018; Ulseth et al. 2019). The exchange of CO_2 between rivers and the atmosphere is in most cases computed from the air-water gradient of the CO_2 concentration and k parameterised as function of stream morphology (e.g. slope or depth) and water flow (or discharge). However, there can be large errors associated to the computation of the dissolved CO_2 concentration from pH and total alkalinity (TA) in particular for low alkalinity waters, so that high-quality direct measurements of dissolved CO_2 concentration are preferred (Abril et al. 2015), although scarce. In the tropics, research on GHGs in rivers has mainly focussed on South American rivers, and in particular on the Central Amazon (Richey et al. 1988; 2002; Melack et al. 2004; Abril et al. 2014; Barbosa et al. 2016; Scofield et al. 2016), while until recently African rivers were nearly uncharted with a few exceptions (Koné et al. 2009; 2010).

There is also a lack of understanding of the drivers of the fluvial concentrations of GHGs, hence, ultimately of the drivers of their exchange with the atmosphere. It is unclear to which extent CO_2 emissions from rivers are sustained by in-situ net

heterotrophy and/or by lateral inputs of CO_2. The global organic carbon degradation by net heterotrophy of rivers and streams given by Battin et al. (2008) of 0.2 PgC yr^{-1} is insufficient to sustain global riverine CO_2 emissions given by the most recent estimates of 0.7-1.8 PgC yr^{-1} (Raymond et al. 2013; Lauerwald et al. 2015),

5   suggesting an important role of lateral CO_2 inputs in sustaining emissions to the atmosphere from rivers. In a regional study in the US, Hotchkiss et al. (2015) estimated that in-stream organic matter degradation could only sustain 14% and 39% of CO_2 riverine emissions in small and large systems, respectively. It is also unclear to which extent CO_2 and CH_4 emissions from rivers are sustained by carbon inputs

10   either from the terrestrial biome (*terra firme*) or from wetlands (flooded forests and macrophytes) (Abril and Borges 2019). This difference has large implications for our fundamental understanding of carbon cycling in rivers and their connectivity with respective catchments, but also, consequently, for our capacity to predict how GHG emissions from rivers might be modified in response to climate change (warming and

15   modification of the hydrological cycle), water diversion (damming, water abstraction) or land use change on the catchment (e.g. Klaus et al. 2018). In upland areas, low order stream CO_2 emissions are undoubtedly related to soil-water and ground-water CO_2 inputs, although CO_2 degassing takes place over very short distances from point sources (≤200 m), is highly variable in space and seasonally, and mainly occurs

20   during short-lived high-flow events that promote shallow flowpaths (e.g. Duvert et al. 2018). Low order streams (1-3) might account for about 1/3 of the global riverine CO_2 emissions (Marx et al. 2017). Recently acquired data-sets allowed to show that inputs from riparian wetlands seem to be of paramount importance in sustaining CO_2 and CH_4 emissions to the atmosphere from large tropical lowland rivers (Abril et al.

25   2014; Borges et al. 2015a,b). About half of the global surface area of wetlands is located in the tropics and sub-tropics (33°N-33°S) and the rest in the Northern Hemisphere (Fluet-Chouinard et al. 2015), and more than half of river surface area is located in the tropics and sub-tropics (Allen and Pavelsky 2018).

     The Congo River (~4400 km length, freshwater discharge ~44,000 m^3 s^{-1}) has

30   a large drainage basin (3.7 10^6 km²) covered by evergreen forest (dense and mosaic) (~67%) and savannah (shrubland and grassland) (~30%), owing to the tropical climate (annual average precipitation of 1530 mm and air temperature of 23.7°C). The Congo basin accounts for 89% of African rainforests. These rainforests are spread between the Democratic Republic of Congo (54%), Gabon (11%), Cameroon

(10%) and the Republic of Congo (10%), the remaining 15% being shared by several other countries. The mean above-ground biomass of the rainforests in Central Africa (43 kg dry biomass (db) m^{-2}) is much higher than the mean in Amazonia (29 kg$_{db}$ m^{-2}) and nearly equals the mean in the notorious high biomass forests of Borneo (44 kg$_{db}$ m^{-2}) (Malhi et al. 2013). Current estimates of carbon transport from the Congo River close to the mouth rank it as the Earth's second largest supplier of organic carbon to the oceans (Coynel et al. 2005). Despite its overwhelming importance, our knowledge of carbon and nutrient cycling in the Congo river basin is limited to some transport flux data from the 1980's, reviewed by Laraque et al. (2009) and a number of more recent small-scale studies (Bouillon et al. 2012; 2014; Spencer et al. 2012; Lambert et al. 2016), in sharp contrast to the extensive and sustained work that has been done on the Amazon river basin (Alsdorf et al. 2016). The Congo basin has a wide range of contrasting tributaries (differing in lithology, soil characteristics, vegetation, rainfall patterns, …), and extensive flooded forests in its central region, the "Cuvette Centrale Congolaise" (CCC), with an estimated flooded cover of 360,000 km^2, for a total surface area of 1,760,000 km^2 (Bwangoy et al. 2010). Extensive peat deposits are present beneath the swamp forest of the CCC, that store belowground 31 PgC of organic carbon, a quantity similar to the above-ground carbon stock of the forests of the entire Congo basin (Dargie et al. 2017). The tributaries partly drain semi-humid catchments with alternating dry and wet seasons on both sides of the Equator, resulting in a relatively constant discharge and water level for the mainstem Congo River (Runge 2008). Hence, the CCC is an extended zone of year-round inundation (Bwangoy et al. 2010), in sharp contrast with other large tropical rivers such as the Amazon where floodplain inundation shows clear seasonality (Hamilton et al. 2002).

Data on dissolved GHGs (CH$_4$, N$_2$O and CO$_2$) have been reported in rivers in the western part of the Congo basin in four major river basins in the Republic of Congo (Alima, Lefini, Sangha, Likouala-Mossaka) (Mann et al. 2014; Upstill-Goddard et al. 2017), and we previously reported GHGs data collected in the eastern part of the basin in the Democratic Republic of Congo in the framework of a broad synthesis of riverine GHGs at the scale of the African continent (Borges et al. 2015a) and of a general comparison of the Congo and the Amazon Rivers (Borges et al. 2015b). Here, we describe in more detail the variability of GHGs based on a data-set collected during 10 field expeditions from 2010 to 2015 (Fig. 1 and 2), in particular

with regards to spatial and seasonal patterns, as well as with regards to the origin of fluvial CO_2 by integrating metabolic measurements (primary production and respiration), stable isotope ratios of dissolved inorganic carbon (DIC), and characteristics of the catchments with regards to the cover of wetlands. Comparison of data obtained in streams within and outside the giant wetland area of the CCC allows a natural large-scale test of the influence of the connectivity of wetlands on CO_2 and CH_4 dynamics in lowland tropical rivers.

2. Material and Methods

2.1. Field expeditions and fixed monitoring

Samples were collected during a total of ten field expeditions (Figs. 1 and 2). Three were done from a medium sized boat (22 m long) on which we deployed the equipment for continuous measurements of the partial pressure of CO_2 (pCO_2) (total n=30,490) as well as the field laboratory for conditioning water samples. Sampling in the mainstem and large tributaries was made from the medium sized boat, while sampling in smaller tributaries was made with a pirogue. These large-scale field expeditions covered twice the Kisangani-Kinshasa transect (03/12/13-19/12/13; 10/06/14-30/06/14), and the Kwa river up to Ilebo (16/04/15-06/05/15). During the other cruises, the field laboratory was installed in a base camp (typically in a village along the river), and travelling and sampling was made with small pirogues on which it was not possible to deploy the apparatus for continuous measurements of pCO_2. Three cruises covered the section from Kisangani to the mouth of the Lomami River (20/11/12-08/12/12; 17/09/13-26/09/13; 13/03/14-21/03/14), one cruise the section from Kisangani to the mouth of the Itimbiri River (08/05/10-06/06/10), and three cruises (previously reported by Bouillon et al. (2012; 2014)) covered the Oubangui river network around the city of Bangui (21-23/03/10; 20-23/03/11; 20-24/11/12).

Fixed sampling was carried out in the Congo mainstem at proximity of the city of Kisangani (10/12/2012-16/04/2018), the Oubangui mainstem at proximity of the city of Bangui (20/03/2010-31/03/2012), the Kasaï mainstem at proximity of the village of Dima close to the city of Bandundu (14/04/2015-15/05/2017). Sampling was carried out at regular intervals, every 15 days in the Congo and Oubangui

mainstems, and every month in the Kasaï mainstem. Data from the Oubangui catchment were previously reported by Bouillon et al. (2012; 2014).

2.2. Continuous measurements

Continuous measurements (1 min interval) of pCO_2 were made with an equilibrator designed for turbid waters (Frankignoulle et al. 2001) coupled to a non-dispersive infra-red gas analyser (IRGA) (Li-Cor 840). The equilibrator consisted of a Plexiglas cylinder (height of 70 cm and internal diameter of 7 cm) filled with glass marbles; pumped water flowed from the top to the bottom of the equilibrator at a rate of about 3 L min^{-1}; water residence time within the equilibrator was about 10 secs, while 99% of equilibration was achieved in less than 120 secs (Frankignoulle et al. 2001). This type of equilibrator system was shown to be the fastest among commonly used equilibration designs (Santos et al. 2012). In parallel to the pCO_2 measurements, water temperature, specific conductivity, pH, dissolved oxygen saturation level (%O_2), turbidity were measured with an YSI multi-parameter probe (6600), and position with a Garmin geographical position system (Map 60S) portable probe. Water was pumped to the equilibrator and the multi-parameter probe (on deck) with a 12V-powered water pump (LVM105) attached on a wooden pole to the side of the boat at about 1 m depth. We did not observe bubble entrainment in water circuit to the equilibrator, as the sailing speed was low (maximum speed 12 km h^{-1}). Instrumentation was powered by 12V batteries that were re-charged in the evening with power generators.

2.3. Discrete sampling

In smaller streams, sampling was done from the side of a pirogue with a 1.7L Niskin bottle (General Oceanics) for gases (CO_2, CH_4, N_2O) and a 5L polyethylene water container for other variables. Water temperature, specific conductivity, pH, and %O_2 were measured in-situ with a YSI multi-parameter probe (ProPlus). pCO_2 was measured with a Li-Cor Li-840 IRGA based on the headspace technique with 4 polypropylene syringes (Abril et al. 2015). During two cruises (20/11/12-08/12/12; 17/09/13-26/09/13, n=38), a PP Systems EGM-4 was used as an IRGA instead of the Li-Cor Li-840. During one of the cruises (13-21/03/2014, n=20) the equilibrated

headspace was stored in pre-evacuated 12 ml Exetainer (Labco) vials and analysed in the home laboratory with a gas chromatograph (GC) (see below). Similarly, the equilibrated headspace was stored in pre-evacuated 12 ml Exetainer (Labco) vials for pCO_2 analysis from the fixed sampling in Kisangani. This approach was preferred to the analysis of pCO_2 from the samples for CH_4 and N_2O analysis, as the addition of $HgCl_2$ to preserve the water sample from biological alteration led to an artificial increase of CO_2 concentrations most probably related to the precipitation of $HgCO_3$ (Fig. S1).

Both YSI multi-parameter probes were calibrated according to manufacturer's specifications, in air for $\%O_2$ and with standard solutions for other variables: commercial pH buffers (4.00 and 7.00), a 1000 μS cm^{-1} standard for conductivity and a 124 nephelometric turbidity unit (NTU) standard for turbidity. The turbidity data from the YSI 6600 compared satisfactorily with discrete total suspended matter (TSM) measurements (Fig. S2), so hereafter we'll refer to TSM for both discrete samples and sensor data. The Li-Cor 840 IRGAs were calibrated before and after each cruise with ultrapure N_2 and a suite of gas standards (Air Liquide Belgium) with CO_2 mixing ratios of 388, 813, 3788 and 8300 ppm. The overall precision of pCO_2 measurements was ±2.0%.

2.4. Metabolism measurements

Primary production (PP) was measured during 2h incubations along a gradient of light intensity using $^{13}C\text{-}HCO_3^-$ as a tracer, as described in detail by Descy et al. (2017). Data were integrated vertically with PAR profiles made with a Li-Cor Li-193 underwater spherical sensor, and at daily scale with surface PAR data measured during the cruises with a Li-190R quantum sensor. In order to extend the number of PP data points we developed a very simple model as function of Chlorophyll-*a* concentration (Chl-*a*) and of Secchi depth (S_d):

$$PP = -4.4 + 0.166 \times S_d + 3.751 \times \text{Chl-}a$$

where PP is in mmol m^{-2} d^{-1}, S_d in cm and Chl-*a* in μg L^{-1}

This approach is inspired from empirical models such as the one developed by Cole and Cloern (1987) that accounts for phytoplankton biomass given by Chl-a, light extinction given by the photic depth and daily surface irradiance. We use S_d as a proxy for photic depth, and in order to simplify the computations, we did not include in the model daily surface irradiance, since it is nearly constant year round in our study site close to the Equator. The model predicts satisfactorily the PP (Fig. S3) except at very low Chl-a values at which the model over-estimates PP (due to the S_d term). In order to overcome this, we assumed a zero PP value for Chl-a concentrations < 0.3 µg L^{-1}.

Pelagic community respiration (CR) was determined from the decrease of O_2 in 60 ml biological oxygen demand bottles (Weathon) over ~24 h incubation periods. The bottles were kept in the dark and close to in-situ temperature in a cool-box filled with in-situ water. The O_2 decrease was determined from triplicate measurements at the start and the end of the incubation with an optical O_2 probe (YSI ProODO). At the end of incubation the sealed samples were homogenised with a magnetic bar prior to the measurement of O_2. Depth integration was made by multiplying the CR in surface waters by the depth measured at the station with a portable depth meter (Plastimo Echotest-II).

For methane oxidation measurements, seven 60 ml borosilicate serum bottles (Weathon) were filled sequentially from the Niskin bottle and immediately sealed with butyl stoppers and crimped with aluminum caps. The butyl stoppers were cleaned of leachable chemicals by boiling in deionized water during 15 minutes in the home laboratory. The first and the last bottle to be filled were then poisoned with a saturated solution of $HgCl_2$ (100 µl) injected through the butyl stopper with a polypropylene syringe and a steel needle, corresponding to the initial concentration of the incubation (T0). The other bottles were stored in a cool-box full of in-situ water (to keep samples close to in-situ temperature and in the dark), and were poisoned approximately 12h after T0 (T1), and then approximately every 24h after T0 (T2, T3, T4 and T5). The difference between the two T0 samples was close to the typical precision of measurements showing that the water was homogeneous within the Niskin bottle with regards to CH_4 concentration, and no measurable loss of CH_4 occurred when filling the seven vials. Methane oxidation was computed from the linear decrease of CH_4 concentration with time.

2.5. Sample conditioning and laboratory analysis

Samples for CH_4 and N_2O were collected from the Niskin bottle with a silicone tube in 60 ml borosilicate serum bottles (Weathon), poisoned with 200 µl of a saturated solution of $HgCl_2$ and sealed with a butyl stopper and crimped with aluminium cap. Measurements were made with the headspace technique (Weiss 1981) and a GC (SRI 8610C) with a flame ionisation detector for CH_4 (with a methanizer for CO_2) and electron capture detector for N_2O calibrated with CO_2:CH_4:N_2O:N_2 gas mixtures (Air Liquide Belgium) with mixing ratios of 1, 10 and 30 ppm for CH_4, 404, 1018, 3961 ppm for CO_2, and 0.2, 2.0 and 6.0 ppm for N_2O. The precision of measurement based on duplicate samples was ±3.9% for CH_4 and ±3.2% for N_2O. The CO_2 concentration is expressed as partial pressure in parts per million (ppm) and CH_4 as dissolved concentration (nmol L^{-1}), in accordance with convention in existing topical literature, and because both quantities were systematically and distinctly above saturation level (400 ppm and 2-3 nmol L^{-1}, respectively). Variations of N_2O were modest and concentrations fluctuated around atmospheric equilibrium, so data are presented as percent of saturation level (%N_2O, where atmospheric equilibrium corresponds to 100%), computed from the global mean N_2O air mixing ratios given by the Global Monitoring Division (GMD) of the Earth System Research Laboratory (ESRL) of the National Oceanic and Atmospheric Administration (NOAA) (https://www.esrl.noaa.gov/gmd/hats/combined/N2O.html), and using the Henry's constant given by Weiss and Price (1982).

The flux (F) of CO_2 (FCO_2), CH_4 (FCH_4) and N_2O (FN_2O) between surface waters and the atmosphere was computed according to Liss and Slater (1974):

$$F = k.\Delta G$$

where k is the gas transfer velocity (cm h^{-1}) and ΔG is the air-water gradient of a given gas.

Atmospheric pCO_2 data from Mount Kenya station (NOAA ESRL GMD) and a constant atmospheric CH_4 partial pressure of 2 ppm were used. Atmospheric mixing ratios given in dry air were converted to water vapor saturated air, using the water vapor formulation of Weiss and Price (1982) as function of salinity and water temperature. The k normalized to a Schmidt number of 600 (k_{600} in cm h^{-1}) were

derived from the parameterisation as a function slope and stream water velocity given by equation 5 of Raymond et al. (2012):

k_{600} = 8.42 + 11838 x VS

5   where V is stream velocity (m s^{-1}) and S is slope (unitless)

We chose this parameterisation because it is based to date on the most exhaustive compilation of k values in streams derived from tracer experiments and was used in the global riverine CO_2 efflux estimates of Raymond et al. (2013) and

10   Lauerwald et al. (2015). Values of V and S were derived from a geographical information system (GIS) as described in section 2.6.

During the June 2014 field expedition, samples for the stable isotope composition of CH_4 ($\delta^{13}C$-CH_4) were collected and preserved similarly as described

15   above for the CH_4 concentration. The $\delta^{13}C$-CH_4 was determined with a custom developed interface, whereby a 20 ml He headspace was first created, and CH_4 was flushed out through a double-hole needle, non-CH_4 volatile organic compounds were trapped in liquid N_2, CO_2 was removed with a soda lime trap, H_2O was removed with a magnesium perchlorate trap, and the CH_4 was quantitatively oxidized to CO_2 in an

20   online combustion column similar to that of an elemental analyzer. The resulting CO_2 was subsequently pre-concentrated by immersion of a stainless steel loop in liquid N_2, passed through a micropacked GC column (Restek HayeSep Q 2m length, 0.75mm internal diameter), and finally measured on a Thermo DeltaV Advantage isotope ratio mass spectrometer (IRMS). Calibration was performed with CO_2

25   generated from certified reference standards (IAEA-CO-1 or NBS-19, and LSVEC) and injected in the line after the CO_2 trap. Reproducibility of measurement based on duplicate injections of samples was typically better than ±0.5 ‰.

The fraction of CH_4 removed by methane oxidation (Fox) was calculated with a closed-system Rayleigh fractionation model (Liptay et al. 1998) according to:

ln(1 - Fox) = [ln($\delta^{13}C$-$CH_{4\_initial}$ + 1000) – ln($\delta^{13}C$-CH_4 + 1000)] / [α - 1]

where δ^{13}C-CH$_{4\_initial}$ is the signature of dissolved CH$_4$ as produced by methanogenesis in sediments, δ^{13}C-CH$_4$ is the signature of dissolved CH$_4$ in-situ, and α is the fractionation factor.

We used a value of 1.02 for α based on field measurements in a tropical lake (Morana et al. 2015). For δ^{13}C-CH$_{4\_initial}$, we used a value of -60.2‰ which we measured in bubbles from the sediment trapped with a funnel in one occasion in a river dominated by *Vossia cuspidata* wetlands (16/04/15-06/05/15). The model we used to compute Fox applies for closed systems, implying that CH$_4$ is assumed not to be exchanged with surroundings in contrast to open system models. Running river water corresponds to a system that is intermediate between closed and open chemical systems, since it is open to the atmosphere and the sediments, but on the other hand the water parcel can be partly viewed as a closed system being transported downstream with the flow. As such, the water parcel receives a certain amount of CH$_4$ from sediments and then is transported downstream away from the initial input of CH$_4$. We also applied two common open-system models to estimate Fox given by Happel et al. (1994) and by Tyler et al. (1997) that have also been applied in lake systems (Bastviken et al. 2002). However, both open-system models gave Fox values > 1 in many cases (data not shown) since the difference between δ^{13}C of the CH$_4$ source and measured δ^{13}C in dissolved CH$_4$ was often much higher than expected from the assumed isotopic fractionation (1.02). The same observation (Fox > 1) was also reported with open-system models in the lakes studied by Bastviken et al. (2002). Since Fox values > 1 are not conceptually possible, we preferred to use instead the results from the closed-system model, although we acknowledge that flowing waters are in fact intermediary systems between closed and open, and that consequently the computed Fox values are likely under-estimated.

Samples for the stable isotope composition of DIC (δ^{13}C-DIC) were collected from the Niskin bottle with a silicone tube in 12 ml Exetainer vials (Labco) and poisoned with 50 µL of a saturated solution of HgCl$_2$. Prior to the analysis of δ^{13}C-DIC, a 2 ml helium headspace was created and 100 µL of phosphoric acid (H$_3$PO$_4$, 99%) was added in the vial in order to convert CO$_3^{2-}$ and HCO$_3^-$ to CO$_2$. After overnight equilibration, up to 1 mL of the headspace was injected with a gastight syringe into a coupled elemental analyser - IRMS (EA-IRMS, Thermo FlashHT or Carlo Erba EA1110 with DeltaV Advantage). The obtained data were corrected for

isotopic equilibration between dissolved and gaseous CO_2 as described by Gillikin and Bouillon (2007). Calibration was performed with certified standards (NBS-19 or IAEA-CO-1, and LSVEC). Reproducibility of measurement based on duplicate injections of samples was typically better than ±0.2 ‰.

5   Water was filtered on Whatman glass fiber filters (GF/F grade, 0.7 µm porosity) for TSM (47 mm diameter), particulate organic carbon (POC) and particulate nitrogen (PN) (25 mm diameter) (precombusted at 450°C for 5h) and Chl-*a* (47 mm diameter). Filters for TSM and POC were stored dry and filters for Chl-*a* were stored frozen at -20°C. Filters for POC analysis were decarbonated with HCl

10   fumes for 4h and dried before encapsulation into silver cups; POC and PN concentration and carbon stable isotope composition (δ^{13}C-POC) were analysed on an EA-IRMS (Thermo FlashHT with DeltaV Advantage), with a reproducibility better than ±0.2 ‰ for stable isotopic composition and better than ±5% for bulk concentration of POC and PN. Data were calibrated with certified (IAEA-600:

15   caffeine) and in-house standards (leucine and muscle tissue of Pacific tuna) that were previously calibrated versus certified standards. The Chl-*a* samples were analysed by high performance liquid chromatography according to Descy et al. (2005), with a reproducibility of ±0.5% and a detection limit of 0.01 µg L^{-1}. Part of the Chl-*a* data were previously reported by Descy et al. (2017).

20   The water filtered through GF/F Whatman glass fibber filters was collected and further filtered through polyethersulfone syringe encapsulated filters (0.2 µm porosity) for stable isotope composition of O of H_2O (δ^{18}O-H_2O), TA, dissolved organic carbon (DOC), major elements (Na^+, Mg^{2+}, Ca^{2+}, K^+ and dissolved silicate (Si)), nitrate (NO_3^-), nitrite (NO_2^-) and ammonium (NH_4^+). Samples for δ^{18}O-H_2O were stored at ambient

25   temperature in polypropylene 8 ml vials and measurements were carried out at the International Atomic Energy Agency (IAEA, Vienna), where water samples were pipetted into 2 ml vials, and measured twice on different laser water isotope analyzers (Los Gatos Research or Picarro). Isotopic values were determined by averaging isotopic values from the last four out of nine injections, along with memory

30   and drift corrections, with final normalization to the VSMOW/SLAP scales by using 2-point lab standard calibrations, as fully described in Wassenaar et al. (2014) and Coplen and Wassenaar (2015). The long-term uncertainty for standard δ^{18}O values was ±0.1‰. Samples for TA were stored at ambient temperature in polyethylene 55 ml vials and measurements were carried out by open-cell titration with HCl 0.1 mol L^-

[1] according to Gran (1952), and data quality checked with certified reference material obtained from Andrew Dickson (Scripps Institution of Oceanography, University of California, San Diego, USA), with a typical reproducibility better than ±3 µmol kg^{-1}. DIC was computed from TA and pCO$_2$ measurements using the carbonic acid

5   dissociation constants for freshwater of Millero (1979) using the CO2sys package. Samples to determine DOC were stored at ambient temperature and in the dark in 40 ml brown borosilicate vials with polytetrafluoroethylene (PTFE) coated septa and poisoned with 50 µL of H$_3$PO$_4$ (85%), and DOC concentration was determined with a wet oxidation total organic carbon analyzer (IO Analytical Aurora 1030W), with a

10   typical reproducibility better than ±5%. Part of the DOC data were previously reported by Lambert et al. (2016). Samples for major elements were stored in 20 ml scintillation vials and preserved with 50 µl of HNO$_3$ (65%). Major elements were measured with inductively coupled plasma MS (ICP-MS; Agilent 7700x) calibrated with the following standards: SRM1640a from National Institute of Standards and

15   Technology, TM-27.3 (lot 0412) and TMRain-04 (lot 0913) from Environment Canada, and SPS-SW2 Batch 130 from Spectrapure Standard. Limit of quantification was 0.5 µmol L^{-1} for Na$^+$, Mg^{2+} and Ca^{2+}, 1.0 µmol L^{-1} for K$^+$ and 8 µmol L^{-1} for Si. Samples were collected during four cruises (08/05/10-06/06/10; 20/11/12-08/12/12; 03/12/13-19/12/13; 16/04/15-06/05/15) for NO$_3^-$, NO$_2^-$ and NH$_4^+$ and were stored

20   frozen (-20°C) in 50 ml polypropylene vials. NO$_3^-$ and NO$_2^-$ were determined with the sulfanilamide colorimetric with the vanadium reduction method (APHA, 1998), and NH$_4^+$ with the dichloroisocyanurate-salicylate-nitroprussiate colorimetric method (SCA, 1981). Detection limits were 0.3, 0.01, and 0.15 µmol L^{-1} for NH$_4^+$, NO$_2^-$ and NO$_3^-$, respectively. Precisions were ±0.02 µmol L^{-1}, ±0.02 µmol L^{-1}, and ±0.1 µmol L^{-1}

25   for NH$_4^+$, NO$_2^-$ and NO$_3^-$, respectively.

2.6. GIS

The limits of the river catchments and Strahler order of rivers and streams

30   were determined from the geospatial HydroSHEDS data-set (https://hydrosheds.cr.usgs.gov/) using ArcGIS® (10.3.1). Land cover data were extracted from the global land cover (GLC) 2009 data-set (http://due.esrin.esa.int/page_globcover.php) from the European Space Agency GlobCover 2009 project for the following classes: Croplands, Mosaic

Cropland/vegetation, Dense forest, Flooded dense forest, Open forest/woodland, Shrublands, Mosaic forest or shrubland/grassland, Grasslands, Flooded grassland, Water bodies. Shrubland and grassland classes were aggregated for the estimate of savannah. Theoretical contribution of C_4 vegetation were extracted based on the vegetation $\delta^{13}C$ isoscape for Africa from Still and Powel (2010) but corrected for agro-ecosystems according to the method of Powell et al. (2012).

The geospatial and statistical methods to compute river width, length, Strahler stream order, surface area, slope, flow velocity, and discharge throughout the Congo River network are described in detail in the Supplemental Information file.

2.7. Statistical analysis

Statistical tests were carried out using GraphPad Prism® software at 0.05 level, and normality of the distribution was tested with the D'Agostino-Pearson omnibus normality test.

3. Results and discussion

The "Results and discussion" section starts by the description of the spatial variations of general limnological variables as well as GHGs along the two main transects (Kinsangani-Kinshasa and Kwa) and as function of stream order and the presence of the CCC. The following sections deal with the seasonal variability and the drivers of CO_2 dynamics, based on one hand on the metabolic measurements and on the other hand on stable isotopic composition of DIC. The final section deal with fluxes of GHGs between the river and the atmosphere, that are presented and discussed firstly as areal fluxes and finally as integrated fluxes at the scale of the basin and at global scale.

3.1. Spatial variations along the Kisangani-Kinshasa transect of general limnological variables and dissolved GHGs

Figures 3 and 4 show the spatial distribution of variables in surface waters of the mainstem Congo River and confluence with tributaries along the Kisangani-Kinshasa transect during high water (HW, December 2013) and falling water (FW,

June 2014) periods (Fig. 1 and 2). Numerous variables show a regular pattern in the mainstem (increase or decrease) due to the gradual inputs from tributaries with a different (higher or lower) value than the mainstem. Specific conductivity, TA, δ^{13}C-DIC, pH, %O_2, %N_2O, TSM, pH, and δ^{18}O-H_2O decreased, while pCO_2 and DOC increased in the mainstem along the Kisangani-Kinshasa transect. Numerous tributaries had black-water characteristics (low conductivity, TA, pH, %O_2, TSM and high DOC) while the mainstem had generally white-water characteristics. The black-water tributaries were mainly found in the region of the CCC, while tributaries upstream or downstream of the CCC had in general more white-water characteristics. The differences between black-waters and white-waters were apparent in the patterns of continuous measurements of pCO_2 showing a negative relationships with %O_2, TSM, pH and specific conductivity (Fig. S4).

Specific conductivity in the mainstem Congo River decreased from 48.3 (HW) / 78.9 (FW) µS cm^{-1} in Kisangani to 26.5 (HW) / 32.7 (FW) µS cm^{-1} in Kinshasa (Figs. 3 and 4). This decreasing pattern was related to a gradual dilution with tributary water with lower conductivities, on average 27.6±9.9 (HW) and 31.9±17.8 (FW) µS cm^{-1}. The lowest specific conductivity was measured in the Lefini River that is part of the Téké plateau, where rain water infiltrates into deep aquifers across thick sandy horizons leading to water with a low mineralisation (Laraque et al. 1998). TA in the mainstem decreased from 344 (HW) / 697 (FW) µmol kg^{-1} in Kisangani to 195 (HW) / 269 (FW) µmol kg^{-1} in Kinshasa, with an average in tributaries of 141±119 (HW) and 136±141 (FW) µmol kg^{-1}. δ^{13}C-DIC roughly followed the patterns of TA, decreasing in the mainstem from -7.9 (HW) / -13.8 (FW) ‰ in Kisangani to -11.8 (HW) / -17.8 (FW) ‰ in Kinshasa, with an average in tributaries of -21.7±3.2 (HW) and -20.9±4.3 (FW) ‰. TSM in the mainstem decreased from 92.9 (HW) / 23.2 (FW) mg L^{-1} in Kisangani to 45.4 (HW) / 18.2 (FW) mg L^{-1} in Kinshasa, with an average in tributaries of 9.3±13.4 (HW) / 8.5±9.3 (FW) mg L^{-1}. The highest TSM values were recorded in the Kwa (44.4 (HW) and 15.8 (FW) mg L^{-1}) and in the Nsele, a small stream draining savannah and flowing into pool Malebo (71.4 (HW) and 34.8 (FW) mg L^{-1}). pH in the mainstem decreased from 6.73 (HW) / 7.38 (FW) in Kisangani to 6.11 (HW) / 6.29 (FW) in Kinshasa, with an average in tributaries of 5.44±0.88 (HW) / 4.91±1.05 (FW). %O_2 values in the mainstem decreased from 89.2 (HW) / 92.6 (FW) % in Kisangani to 57.8 (HW) / 79.7 (FW) % in Kinshasa, with an average in tributaries of 36.7±33.3 (HW) / 43.7±35.8 (LW) %. DOC increased from 5.9 (HW) / 5.1 (FW) mg L^{-1} in

Kisangani to 11.9 (HW) / 9.4 (FW) mg L^{-1} in Kinshasa, with an average in tributaries of 16.1±10.6 (HW) / 17.9±15.2 (FW) mg L^{-1}. Extremely low pH values were recorded in rivers draining the CCC, with values as low as 3.6, coinciding with nearly anoxic conditions (%O_2 down to 0.3 %) in surface waters and very high DOC content (up to

5   67.8 mg L^{-1}). δ^{18}O-H_2O in the mainstem decreased from -2.2 (HW) / -1.6 (FW) ‰ in Kisangani to -2.9 (HW) / -2.2 (FW) ‰ in Kinshasa, with an average in the tributaries of -2.7±0.9 (HW) / -2.2±0.8 ‰. Temperature increased in the mainstem from 26.0 (HW) / 27.1 (FW) °C in Kisangani to 27.8 (HW) / 27.3 (FW) °C in Kinshasa, due to exposure in the uncovered mainstem to solar radiation, as temperature was lower in

10   tributaries with an average of 26.0±1.1 (HW) / 26.1±1.7 (FW) °C due to more shaded conditions (forest cover).

The pCO_2 values in the mainstem increased from 2424 (HW) / 1670 (FW) ppm in Kisangani to 5343 (HW) / 2896 (FW) ppm in Kinshasa, with an average in tributaries of 8306±4089 (HW) / 8039±5311 (FW) ppm. pCO_2 in tributaries was in

15   general higher than in the mainstem with a few exceptions, namely in rivers close to Kinshasa (1582 to 1903 (HW) and 1087 to 2483 (FW) ppm), due to degassing at water falls upstream of the sampling stations, as the terrain is more mountainous in this area than in more gently sloping catchments upstream, and also possibly due to a larger contribution of savannah to the catchment cover. The highest pCO_2 values

20   (up to 16,942 ppm) were observed in streams draining the CCC. CH_4 in the mainstem decreased from 85 (HW) / 63 (FW) nmol L^{-1} in Kisangani to 24 (HW) / 22 (FW) nmol L^{-1} just before Kinshasa, and then increased again in the Malebo pool (82 (HW) / 78 (FW) nmol L^{-1}) possibly related to the shallowness (~3 m in Malebo pool versus ~30 m depth at station just upstream). The general decreasing pattern of CH_4

25   in the mainstem resulted from CH_4 oxidation, as indicated by ^{13}C enriched values in the mainstem (-38.1 to -49.4 ‰) with regards to sediment CH_4 (-60.2 ‰), and the increasing ^{13}C enrichment along the transect (Fig. 5). The calculated fraction of oxidized CH_4 ranged between 0.43 and 0.68 in the mainstem and also increased downstream along the transect (Fig. S5). CH_4 in the tributaries showed a very large

30   range of CH_4 concentration (68 to 51,839 nmol L^{-1} (HW) and 102 to 56,236 nmol L^{-1} (FW)). CH_4 in the tributaries showed a variable degree of ^{13}C enrichment compared to sediment CH_4 (δ^{13}C-CH_4 between -19.3 and -56.3 ‰, Fig. 5), and the calculated fraction of oxidized CH_4 ranged between 0.18 and 0.88 (Fig. S5). Unlike the large rivers of the Amazon where a loose negative relation has been reported (Sawakuchi

et al. 2016), the $\delta^{13}C-CH_4$ values in the Congo River were unrelated to dissolved CH_4 concentrations, and a relatively high ^{13}C enrichment ($\delta^{13}C-CH_4$ up to -19.3 ‰) was observed even at high CH_4 concentrations (correspondingly 3,118 nmol L^{-1}) (Fig. 5). This lack of correlation between concentration and isotope composition of CH_4 was

5   probably related to spatial heterogeneity of sedimentary (and corresponding water column) CH_4 content over a very large and heterogeneous sampling area. The highest CH_4 concentrations were observed at the mouths of small rivers in the CCC. At the confluence with the Congo mainstem, the flow is slowed down leading to the development of shallow delta-type systems with very dense coverage of aquatic

10   macrophytes (in majority *Vossia cuspidata* with a variable contribution of *Eichhornia crassipes,* but also other species, Fig. S6). Such sites are favourable for intense sediment methanogenesis, but due to the stable environment related to near stagnant waters, also very favourable for the establishment of a stable methanotrophic bacterial community in the water column and associated to the root

15   system of floating macrophytes that sustain intense methane oxidation (Yoshida et al. 2014; Kosten et al. 2016). Indeed, we found a very strong relation between CH_4 oxidation and CH_4 concentration on a limited number of incubations carried out in the Kwa river network in April 2015 (Fig. S7). Such conditions can explain the apparently paradoxical combination of high CH_4 concentrations in some cases associated to a

20   high degree of CH_4 oxidation. Microbial oxidation of CH4 might also explain the occurrence of samples with extremely ^{13}C depleted POC ($\delta^{13}C-POC$ down to -39.0 ‰) observed in low $\%O_2$ and high CH_4 environments (Fig. 6) located in small streams of the CCC, that were also characterised by low POC and TSM values (not shown), and high POC:Chl-*a* ratios (excluding the possibility that *in-situ* PP would be

25   at the basis of the ^{13}C-depletion). This suggests that in these environments poor in particles (typical of black-water streams) but with high CH_4 concentrations, methanotrophic bacteria which are able to incorporate ^{13}C-depleted CH_4 into their biomass contribute substantially to POC. While such patterns have been reported at the oxic-anoxic transition zone of lakes with high hypolimnic CH_4 concentrations such

30   as Lake Kivu (Morana et al. 2015), this has never been reported in surface waters of rivers.

      $\%N_2O$ decreased from 198 (HW) / 139 (FW) % in Kisangani to 168 (HW) / 153 (FW) % in Kinshasa, and in most cases $\%N_2O$ was lower in tributaries, on average 114±73 (HW) / 120±69 (FW) %. The under-saturation in N_2O was observed in

streams with high DOC, low $\%O_2$ and relatively low NO_3^-, and most probably related to denitrification of N_2O as also reported in the Amazon river (Richey et al. 1988), and in temperate rivers (Baulch et al. 2011). Denitrification could have occurred in river sediments or soils, although the lowest $\%N_2O$ (and $\%O_2$) occurred in the CCC dominated by flooded soils in the flooded forest. Indeed, there was a general negative relationship between $\%N_2O$ and $\%O_2$ (Fig. 7), with an average $\%N_2O$ of 78.5±59.3% for $\%O_2 < 25\%$ and an average $\%N_2O$ of 155.7±57.7% for $\%O_2 > 25\%$ (Mann-Whitney $p<0.0001$). The decreasing pattern of NH_4^+:DIN and increasing pattern of NO_3^-:DIN with $\%O_2$ indicated the occurrence of nitrification in oxygenated (typical of high Strahler stream order) rivers and prevalence of NH_4^+ in the more reducing and lower oxygenated (typical of low Strahler order) streams in particular draining the CCC, where NO_3^- was probably also removed from the water by sedimentary or soil denitrification (Fig. 7). In addition, in black-water rivers/streams, low pH (down to 4) might have led to the inhibition of nitrification (Le et al. 2019), and also contributed higher NH_4^+:DIN values. Furthermore, the positive relation between $\%N_2O$ and NO_3^-:DIN and the negative relation between $\%N_2O$ and NH_4^+:DIN (Fig. 8) support the hypothesis of N_2O removal by denitrification in O_2-depleted environments (either in stream sediments or soils) while in more oxygenated rivers, N_2O was produced by nitrification. In the mainstem of the Congo, there might be in addition a loop of nitrogen recycling (ammonification-nitrification) sustained by phytoplankton growth and decay, that contributed to maintain over-saturation of N_2O with respect to atmospheric equilibrium, as phytoplankton growth was only observed in the mainstem (Descy et al. 2017). The generally low $\%N_2O$ values in the Congo River network were probably due to the near pristine nature of these systems with low NH_4^+ (2.3±1.3 µmol L^{-1}) and NO_3^- (5.6±5.1 µmol L^{-1}) levels, typical of rivers and streams draining a large fraction (~70%) of forests. Croplands only represented at most 17% on average of the land cover of the studied river catchments, where traditional agriculture is practised with little use of artificial fertilizers. This corresponds to an upper bound of cropland surface area since it was estimated aggregating the "cropland" and "mosaic cropland/vegetation" GLC 2009 categories, the latter corresponding to mixed surfaces with <50% of cropland. The "cropland" GLC 2009 category only accounts for 0.1% on average of the land cover of the studied river catchments. Nitrogen inputs from waste water can also sustain N_2O production in impacted rivers and streams (Marwick et al. 2014), but the largest cities along the

Congo River mainstem are of relatively modest size such as Kisangani (1,600,000 habitants) and Mbandaka (350,000 habitants), especially considering the large dilution due to the massive discharge of the mainstem (sampling was done upstream of the influence of the megacity of Kinshasa with 11,900,000 habitants).

5   The input of the Kwa led to distinct changes of TA and δ^{18}O-H$_2$O (decrease) and TSM (increase) of mainstem values (comparing values upstream and downstream of the Kwa mouth) (Figs 3-4). In the mainstem, continuous measurements of pCO$_2$, pH, %O$_2$, and conductivity showed more variability compared to discrete samples acquired in the middle of channel, in particular in the

10 region of CCC (Figs 3-4). These patterns were related to gradients across the section of channel, as the boat sailed either along the mid-channel or closer to shore. The water from the tributaries flowed along the river banks and did not mix with mainstem middle channel waters, as visible in natural colour remote sensed images (Fig. S8), leading to strong gradients across the section of mainstem channel. During the June

15 2014 field expedition, this was investigated in more detail by a series of six transects perpendicular to the river mainstem channel (Fig. 9). In the upper part (1590 km from Kinshasa), the variables showed little cross-section gradients except for a decrease of conductivity towards the right bank due to inputs from the Lindi River that had distinctly lower specific conductivities (27.2 (HW) / 35.1 (FW) µS cm^{-1}) than the main

20 stem (48.3 (HW) / 78.9 (FW) µS cm^{-1}). At 795 km from Kinshasa, marked gradients appeared in all variables with the presence of black-water characteristics close to the right bank (higher pCO$_2$, and lower %O$_2$, pH, specific conductivity, temperature and TSM values). This feature was related to inputs from large right bank tributaries such as the Aruwimi and the Itimbiri (Table S1). Upstream of this section the only major

25 left-bank tributary is the Lomami that had white-water characteristics, relatively similar to those of the mainstem (Figs. 3-4). The presence of black-water characteristics became apparent also on the left-bank, from cross-sections at 307 and 254 km upstream of Kinshasa, where the river is particularly wide (> 6 km wide), and received the inputs from the Ruki, the second largest left-bank tributary (Table

30 S1) with black-water characteristics. The cross section gradients became less marked at 203 km upstream from Kinshasa, as in this region the river becomes more narrow (2 km wide) leading to increased currents and more lateral mixing. The cross-section gradients nearly disappeared at 158 km upstream of Kinshasa (and 30 km downstream of the Kwa mouth) due to homogenisation by the large Kwa inputs

(nearly 20% of total freshwater discharge from Congo River, Table S1) into a relatively narrow river section (~ 1 km).

3.2. Spatial variations along the Kwa transect

Spatial features of biogeochemical variables along the transect in the Kwa River network (Fig. 10) showed some similarities with two Kisangani-Kinshasa transects along the Congo mainstem (Figs 3-4). The mainstem Kwa had a higher specific conductivity than tributaries (25.1±4.2 versus 21.2±11.5 µS cm^{-1}), higher TA

10   (281±64 vs. 119±118 µmol kg^{-1}), higher temperatures (27.7±0.7 versus 26.3±2.2 °C), higher TSM (40.1±8.9 versus 15.2±35.1 mg L^{-1}), higher pH (6.1±0.2 versus 4.5±0.7), higher %O$_2$ (67.0±7.0 versus 37.9±26.8 %), higher δ^{13}C-DIC (-16.5±1.2 versus -22.6±3.4 ‰), and lower DOC (5.2±1.4 versus 13.0±8.5 mg L^{-1}). Unlike the Kisangani-Kinshasa transects along the Congo mainstem, the δ^{18}O-H$_2$O was lower in the

15   mainstem Kwa (-4.3±0.3 ‰) than in the tributaries (-3.3±0.6 ‰). Note that both the main upstream branches of the Kwa (Kasai and Sankuru) had low δ^{18}O-H$_2$O values. The δ^{18}O-H$_2$O values of the upper Kasai and Sankuru (-4.4 and -4.7 ‰, respectively) were lower than those of the Lualaba (Congo at Kisangani) (-2.2 (HW) / -1.6 (FW) ‰). This was probably related to the lower evapotranspiration over the catchments of

20   the upper Kasai and Sankuru than those of Lualaba (Bultot 1972), leading to more ^{18}O-depleted water (e.g. Simpson and Herczeg 1991). Additionally, the catchment of Kwa has a high fraction of unconsolidated sedimentary (41.4%) and siliciclastic sedimentary (44.3%) rocks than the catchment of the Lualaba that is dominated by metamorphic rocks (68.4%) Unconsolidated sedimentary and siliciclastic sedimentary

25   rocks are more favourable to the infiltration of water and development of aquifers that will minimize evaporation and ^{18}O enrichment, unlike catchments dominated by metamorphic rocks. Note that the tributaries with the lowest δ^{18}O-H$_2$O values were situated downstream of the Kwa and upstream of Kinshasa (Figs. 3-4) and are part of the Téké plateau. These rivers are fed by deep aquifers derived from infiltration of

30   rain through sandy soils (Laraque et al. 1998).

Another difference with the Kisangani-Kinshasa transects along the Congo mainstem, relates to N$_2$O values that were closer to saturation in the Kwa mainstem (110.1±8.8 %), while surface waters oscillated from under-saturation to oversaturation in the tributaries (122.4±59.5 %). This difference could be due to

variations in biogeochemical cycling or in physical settings leading to changes in k. The latter seems more likely due to the strong flow in the Kwa that probably led to high gas transfer velocities and strong degassing of N_2O to the atmosphere. In the Kwa mainstem, pCO_2 (3473±974 ppm) and CH_4 (255±150 nmol L^{-1}) values were

5 lower than in tributaries (8804±5108 ppm, 6,783±16,479 nmol L^{-1}). The highest pCO_2 and CH_4 values of the entire data-set in the Congo River network were observed in a tributary of the Fimi (22,899 ppm and 71,428 nmol L^{-1}) that is bordered by very extensive meadows of the aquatic macrophyte *Vossia cuspidate*, and unrelated to inputs from the shallow Lake Mai Ndombé that showed lower pCO_2 and CH_4 values

10 (3,143 ppm and 250 nmol L^{-1}, respectively).

3.3. Spatial variations as function of stream order and as function of the influence of the CCC

15 The large differences in pCO_2, CH_4, $\%O_2$ and $\%N_2O$ (Figs 3,4,10) among the various sampled tributaries of the Congo River can be analysed in terms of size classes as given by Strahler order (Fig. 11). There were distinct patterns in CH_4 and pCO_2 versus Strahler order, with a decrease of the central value (median and average) for both quantities as a function of Strahler order in streams draining and

20 not draining the CCC (Fig. 11). For nearly all the stream orders, the streams draining the CCC had significantly higher pCO_2 and CH_4 values than streams not draining the CCC (Fig. 11). The $\%O_2$ values per Strahler order did not show any distinct pattern (increase or decrease) in the streams not draining the CCC, but the streams draining the CCC showed an increasing pattern as a function of Strahler order. The $\%O_2$

25 values were significantly lower in the streams draining the CCC than those not draining the CCC (Fig. 11). For $\%N_2O$, the tendency of the central value (median and average) as function of Strahler order did not show a clear pattern for streams not draining the CCC, however, there was a clear increasing pattern with Strahler order for streams draining the CCC. In addition, the $\%N_2O$ values were significantly lower

30 for half of the cases, in streams draining the CCC compared to those not draining it (Fig. 11).

In US rivers, a decreasing pattern as function of Strahler order has previously been reported for pCO_2 (Butman and Raymond 2001; Liu and Raymond 2018). This has been interpreted as reflecting inputs of soil-water enriched in terrestrial respired

CO_2 that have a stronger impact in smaller and lower Strahler order systems, in particular headwater streams, followed by degassing of CO_2 in higher Strahler order rivers (Hotchkiss et al. 2015), although soil-water CO_2 inputs in headwater streams are seasonally variable and spatially heterogeneous (Duvert et al. 2018).

5 Nevertheless, all of the low Strahler order streams we sampled were in lowlands, so, the decreasing pattern of pCO_2 as function of Strahler order could alternatively reflect the stronger influence of riparian wetlands on smaller streams, rather than larger systems. The mechanism remains the same, a high ratio of lateral inputs to water volume in small streams, that is related to soil-water in temperate streams such as in

10 the US but related in addition to riparian wetlands in tropical systems such as those sampled in the Congo River network.

The influence of riparian wetlands on stream pCO_2, CH_4 and %N_2O can be also highlighted when data were separated into rivers draining or not draining the CCC but aggregating into systems smaller or larger than Strahler order 5 to account

15 simultaneously for the effect of stream size (Fig.12). The pCO_2 values were statistically higher in rivers draining the CCC than those not draining it, with median values more than 2 fold higher in both small and large rivers. Conversely, %O_2 levels were statistically lower in rivers draining the CCC than those not draining it, with median values 11 and 2 fold lower in small and large rivers, respectively. Additional

20 evidence on the influence of the connectivity of wetlands with rivers in sustaining high pCO_2 and low %O_2 values was provided by the positive relationship between pCO_2 and flooded dense forest cover and the converse negative relationship between %O_2 and flooded dense forest cover (Fig. 13). These patterns were also consistent with the positive relation between DOC concentration and flooded dense forest reported

25 by Lambert et al. (2016). Note that aquatic macrophytes (*Vossia cuspidata*) most probably also strongly contributed in addition to flooded forest to high pCO_2 and low %O_2 levels, based on *de-visu* observations of dense coverage (Fig S9), although macrophytes have not been systematically mapped and GIS data are unavailable (as for flooded dense forest).

30 Wetlands coverage had also a major importance on CH_4 distribution, as the CH_4 values were statistically higher in rivers draining the CCC than those not draining it (Fig. 12), with median values 10 and 2 fold higher in small and large rivers, respectively. %N_2O were also statistically lower in rivers draining the CCC than those not draining it, with median values 2.7 fold lower in small rivers but 1.4 fold higher in

large rivers. The pattern of %N_2O followed the one of %O_2, and the very low to null N_2O values were observed in the systems draining the CCC where the lowest %O_2 values (close to 0) were also observed due to sedimentary or soil organic matter degradation leading to a decrease of O_2 and N_2O in surface waters (consumption of N_2O by denitrification).

The CH_4:CO_2 molar ratio ranged between 0.0001 and 0.1215, with a mean of 0.0097±0.018. Such ratios were distinctly higher than those typically observed in marine waters (0.0005) and in the atmosphere (0.005). The CH_4:CO_2 molar ratio strongly increased with the decrease of %O_2 and was significantly higher in small rivers draining the CCC (Fig. 13). These patterns were probably related to inputs of organic matter from wetlands and in particular aquatic macrophytes that lead to important organic matter transfer to sediments and high sedimentary degradation of organic matter. This lead to %O_2 decrease in surface waters and a large fraction of organic matter degradation by anaerobic processes compared to aerobic degradation, leading to an increase of the CH_4:CO_2 ratio. The decrease of O_2 and increase of CO_2 in the water in presence of floating macrophytes was probably in part also related to autotrophic root respiration and not fully related to microbial heterotrophic respiration.

3.4. Drivers of CO_2 dynamics – metabolic measurements and daily variations of CO_2

We compared the balance of depth-integrated planktonic PP to water column CR and compared it to FCO_2 to test if *in-situ* net heterotrophy was sufficient to sustain the emissions of CO_2 to the atmosphere (Fig. 15), or if alternatively fluvial CO_2 had a lateral origin (soils or wetlands). A detailed description of spatial and seasonal variations of PP as well as main phytoplankton communities is given by Descy et al. (2017). In brief, phytoplankton biomass was mainly confined to the mainstem and was low in most tributaries. The PP values in the Congo River ranged between 0.0 and 57.5 mmol m^{-2} d^{-1} and were higher than previously reported in tropical river channels, whereas in other tropical rivers phytoplankton production mainly occured in the floodplain lakes. This is due to generally lower TSM values in the Congo and to its relative shallowness that allows net phytoplankton growth in the mainstream unlike other deeper and more turbid tropical rivers such as the Amazon.

Measured PP was 3 out 49 times lower than CR, and on average the PP:CR ratio was 0.28. Volumetric rates of CR ranged between 0.7 and 46.6 mmol m^{-3} d^{-1}, while integrated rates of CR ranged between 3.1 and 790.4 mmol m^{-2} d^{-1}. CR was unrelated to TSM, POC, NH$_4^+$ and Chl-a, but showed a positive relation with DOC,

5   after binning the data (Fig. S10). The same pattern emerged when using modelled PP, to extend the number of data points, with PP 2 out 169 times higher than CR, and on average a PP:CR ratio of 0.15. This indicates that a generalised and strongly net heterotrophic metabolism was encountered in the sampled sites. Yet, in 174 out 187 cases, FCO$_2$ was higher than CR and in 162 out 169 cases, FCO$_2$ was higher

10   than net community production (NCP). CR averaged 81 mmol m^{-2} d^{-1}, and NCP averaged -75 mmol m^{-2} d^{-1} and the corresponding average FCO$_2$ was 740 mmol m^{-2} d^{-1}. The FCO$_2$:CR ratio was higher in lower order streams than higher order streams, with median values ranging between 21 and 139 in stream orders 2-5 and between 3 and 17 in stream orders 6-10 (Fig. 16). This indicates a prevalence of lateral CO$_2$

15   inputs either from soil-water or riparian wetlands in sustaining FCO$_2$ in lower order streams than higher order streams where in-stream CO$_2$ production from net heterotrophy is more important. These patterns are in general agreement with the conceptual framework developed by Hotchkiss et al. (2015), although lateral CO$_2$ inputs were exclusively attributed by these authors to soil-water or ground-water

20   inputs and riparian wetlands were not considered. These patterns are also in agreement with the results reported by Ward et al. (2018) who show that in large high-order rivers of the lower Amazon, in-stream production of CO$_2$ from respiration is sufficient to sustain CO$_2$ emissions to the atmosphere.

        CR was estimated from measurements of O$_2$ concentration decrease in bottles

25   that were not rotated, and this has been shown to lead to an under-estimation of CR up to a factor of two (Richardson et al. 2013; Ward et al. 2018). The under-estimation of our CR measurements due to the absence of rotation is most likely not as severe as in the Richardson et al. (2013) and Ward et al. (2018) studies, as the organic matter in our samples was mostly in dissolved form (median DOC of 8.6 mg L^{-1}), with

30   a low particulate load (median TSM of 14 mg L^{-1} and POC of 1.3 mg L^{-1}), while the median of TSM at the sites studied by Ward et al. (2018) in the Amazon was higher (28.5 mg L^{-1} based on data reported by Ward et al. 2015). We acknowledge that our CR measurements might be under-estimated due to bottle effects and lack of rotation up to a factor of 2 based on the studies of Richardson et al. (2013) and Ward et al.

(2018), nevertheless, it seems unrealistic to envisage an under-estimation of CR by a factor 10 that would allow reconciling the CR (and NCP) estimates with those of FCO_2. Although we did not measure sediment respiration, the average value reported by Cardoso et al. (2014) of 21 mmol m^{-2} d^{-1} for tropical rivers and streams does not

5   allow accounting for the imbalance between FCO_2 and NCP. This then suggests that the emission of CO_2 from the Congo lowland river network is to a large extent sustained by lateral inputs rather than by in-stream production of CO_2 by net heterotrophy. It remains to be determined to which extent this lateral input of CO_2 is sustained by riparian wetlands or soil-groundwater from *terra firme*.

10   The low PP:CR ratio of 0.15 to 0.28 on average, and generally low PP values (on average 12 mmol m^{-2} d^{-1}) were also reflected in the low diurnal variations of pCO_2. We did not carry out dedicated 24 h cycles to look at the day-night variability of pCO_2, due to lack of opportunity given the important navigation time to cover large distances, but we compared the data acquired at the anchoring site on shore

15   (typically around 17h00 universal time (UT), just before dusk) with the data on the same spot the next day (typically around 04h30 UT, just after dawn) (Fig. S11). Unsurprisingly, water temperature measured just before dusk was significantly higher than just after dawn (on average 0.5°C higher), while specific conductivity was not significantly different, indicating that the same water mass was sampled at dusk and

20   dawn (Fig. S11). The pCO_2 and O_2 concentration measured just before dusk were not significantly different than just after dawn, showing that daily variability in these variables was low (Fig. S11). The difference between pCO_2 at dusk and dawn ranged between -2307 and 1186 ppm, and averaged 39 ppm (*n*=39). The wide range of values of the difference of pCO_2 at dusk and at dawn might reflect occasional small

25   scale variability of pCO_2, as the boat anchored for the night close to shore, and frequently at proximity of riparian vegetation. Nevertheless, the average difference is not of the expected sign (in the case of a strong diurnal change of pCO_2 due to PP and CR, pCO_2 should have been lower at dusk than dawn, so difference should have been negative). This difference was also very small compared to the overall range of

30   spatial variations of pCO_2 (1,087 to 22,899 ppm). Day-night variations of pCO_2 have been reported in temperate headwater and low order streams and in one lowland river with an amplitude from ~50 to ~700 ppm (Lynch et al. 2010; Dinsmore et al. 2013; Peter et al. 2014; Crawford et al. 2017; Reiman and Xu 2019), although daily signals of pCO_2 were not systematically observed, and were absent for instance in

streams covered by forest canopy (Crawford et al. 2017). In a low turbidity and very shallow low order stream of the Tana River network, Tamooh et al. (2013) reported on one occasion day-night variation of pCO_2 with an amplitude of ~400 ppm, and in the Zambezi river, during the dry season corresponding to very low TSM values (<10 mg L^{-1}), Teodoru et al. (2015) reported day-night pCO_2 variation in the range of 475 ppm. In both cases, the day-night variations were also small compared to spatial variations of 300 to 5,204 ppm in the Tana and 300 to 14,004 ppm in the Zambezi. In floodplain lakes of the Amazon, daily variations of pCO_2 can be intense (with an amplitude up to ~2,000 ppm) during cyanobacterial blooms (Abril et al. 2013; Amaral et al. 2018), but have not been documented in the river channels of the Amazon. Our data show that in nutrient poor and light limited lowland tropical rivers such as the Congo River, where pelagic PP is low, day-night variations of pCO_2 were negligible compared to spatial variations of pCO_2. We conclude that accounting for night-day variations of pCO_2 should not lead to a dramatic revision of global CO_2 emissions, unlike the recently claim based on data from a lowland temperate river by Reiman and Xu (2019), given that tropical rivers account for 80% of CO_2 emissions (Raymond et al. 2013; Borges et al. 2015a,b; Lauerwald et al. 2015).

3.5.   Drivers of CO_2 dynamics – stable isotopic composition of DIC

The stable isotope composition of DIC can provide information on the origin of CO_2, although the signal depends on the combination of the biological processes that remove or add CO_2 to the water column (CR and PP), rock weathering that adds HCO_3^-, and outgassing which removes CO_2 that is ^{13}C-depleted relative to HCO_3^-. The variable contribution to DIC in time and in space of CO_2 relative to HCO_3^- complicates the interpretation of δ^{13}C-DIC data. The stable isotopic composition of DIC due to rock weathering will depend on the type of rock (silicate or carbonate) and on the origin of the CO_2 involved in rock dissolution (either CO_2 from the atmosphere or from respiration of soil organic matter). The stable isotopic composition of DIC due to the degradation of organic matter will depend in part on whether the organic matter is derived from terrestrial vegetation following the C_3 photosynthetic pathway (woody plants and trees, temperate grasses; δ^{13}C ~ -27‰) compared to the less fractionating C_4 photosynthetic pathway (largely tropical and subtropical grasses; δ^{13}C ~ -13‰) (Hedges et al. 1986; Bird et al. 1994). Spatial and temporal changes of δ^{13}C are

related to the change of the relative abundance of HCO_3^- over CO_2. The degassing of CO_2 to the atmosphere and the addition of HCO_3^- from rock weathering lead to $\delta^{13}C$-DIC values becoming dominated by those related to HCO_3^-. Since CO_2 is isotopically depleted relative to HCO_3^-, CO_2 degassing leads to a gradual enrichment of the

5   remaining DIC pool (e.g. Doctor et al. 2008; Deirmendjian and Abril 2018). The combination of these processes can lead to spatial changes of $\delta^{13}C$-DIC that co-vary with CO_2 and HCO_3^- concentrations. For instance, in the Tana River network, an altitudinal gradient of $\delta^{13}C$-DIC was attributed to a downstream accumulation of HCO_3^- due to rock weathering combined to CO_2 degassing (Bouillon et al. 2009;

10   Tamooh et al. 2003). Figure 17 shows $\delta^{13}C$-DIC as a function of the TA:DIC ratio in the rivers and streams of the Congo, with a general increase of $\delta^{13}C$-DIC from TA:DIC=0 (all of the DIC is in the form of CO_2) towards TA:DIC=1 (nearly all of the DIC is in the form of HCO_3^-). This pattern reflects the mixing of two distinct types of rivers and streams: the lowland systems draining the CCC with low rock weathering

15   due to dominance of deep organic soils (low HCO_3^-) and high CO_2 from respiration leading to TA:DIC close to 0 with low $\delta^{13}C$-DIC, and the systems draining highland regions (Lualaba and Kasaï) with high rock weathering and lower generation of CO_2 from respiration and/or higher CO_2 degassing leading to TA:DIC close to 1 with high $\delta^{13}C$-DIC. The plots of TA:Na^+ and Mg^{2+}:Na^+ versus Ca^{2+}:Na^+ (Fig. 18) showed

20   aggregation of data close to what would be expected for silicate rock weathering based on the average values proposed by Gaillardet et al. (1999). This is in agreement with the dominance of silicate rocks over carbonate rocks in the Congo basin (Nkounkou and Probst 1987). Note that TA values from the Congo are generally very low compared to other large rivers globally (Meybeck 1987), due to the

25   large proportion of relatively insoluble rocks on the catchment (70% of metamorphic rocks) and a small proportion of low soluble rocks such as siliciclastic sedimentary rocks (10% mainly as sand stone), unconsolidated sediments (17% as sand and clays), and a very small proportion of high soluble volcanic rocks (1%). The high TA values in the Lualaba are due to a larger proportion of volcanic rocks in high altitude

30   areas, such as the Virunga region that is rich in volcanic rocks (including basalts) and has been shown to be a hotspot of chemical weathering (Balagizi et al. 2015).

At TA:DIC=0, the $\delta^{13}C$-DIC values are exclusively related to those of CO_2 and might be indicative of the source of mineralized organic matter. The $\delta^{13}C$-DIC values ranged between -28.2 and -15.9 ‰, and averaged -24.1 ‰ (Fig. 17) indicating that

CO$_2$ was produced from the degradation of mixture of organic matter from C$_3$ and C$_4$ origin. Furthermore, δ^{13}C-DIC was positively related to pCO$_2$ (Fig. 17), indicating that in the streams with high pCO$_2$ values, the CO$_2$ was generated from the degradation organic matter with a higher contribution from C$_4$ plants. The δ^{13}C-DIC values were

5   unrelated to the contribution of C$_4$ vegetation on the catchment (*terra firme*), as modelled by Still and Powell (2010), and the cover by savannah on the catchment given by GLC2009 (Fig. S12). Further, the most enriched δ^{13}C-DIC values (>-21 ‰), corresponded on average to a low contribution of C$_4$ vegetation on the catchment (7.4%), and low contribution of savannah cover on the catchment (0.8%). These

10   patterns are inconsistent with an origin from *terra firme* of the C$_4$ material that led to high pCO$_2$ in streams (Fig. 17) , but is rather more consistent with a larger contribution of degradation of C$_4$ aquatic macrophyte material in high CO$_2$ streams.

3.6. Seasonal variations

The difference between the HW and FW in the mainstem along the Kisangani-Kinshasa transects (Fig. 3 and 4) were relatively modest with higher specific conductivity, TA, δ^{13}C-DIC and TSM (at Kisangani), biogeochemical signatures of higher surface run-off during the HW sampling (December 2013) and water flows

20   from deeper soil horizons (or ground-water) during the FW sampling (June 2014). The comparison of tributaries that were sampled during both HW and FW periods along the Kisangani-Kinshasa transects shows that pCO$_2$ was significantly higher (Wilcoxon match-pairs signed rank test p=0.078) during HW for large systems (freshwater discharge ≥ 300 m^3 s^{-1}, Table S1) but not significantly different for small

25   systems (freshwater discharge < 300 m^3 s^{-1}), irrespective whether left or right bank (Fig. 19). However, no significant differences among the HW and FW periods occurred in %O$_2$, CH$_4$ and %N$_2$O for either small of large systems, irrespective whether left or right bank (Fig. 19). This indicates that across the basin, spatial differences among tributaries are more important than seasonal variations within a

30   given tributary. The average difference for large rivers between HW and FW was on average only 1,745 ppm for pCO$_2$ when the respective range of variation for the whole data-set was from 1,087 to 22,899 ppm.

Yearly cycles of CH$_4$ and N$_2$O were established on the Lualaba (6 yrs), the Oubangui (2yrs) and the Kasaï (2 yrs) (Figs. 20 and 21), while pCO$_2$ is only available

during 2 yrs in the Lualaba. In the Oubangui and the Kasaï, CH_4 concentration peaked with the onset of rising water and decreased as water level continued to increase. The decrease of CH_4 as discharge peaked in the Oubangui and the Kasaï is most probably related to dilution by surface runoff as also testified by the decrease

5   of specific conductivity and TA (not shown). The increase at the onset of rising water could be related to initial flushing of soil atmosphere enriched in CH_4 as rain penetrates superficial layers of soils. In the Lualaba the CH_4 seasonal variations seem to follow more closely those of freshwater discharge (for instance in 2014). Unlike the Kasaï and the Oubangui, the Lualaba has very extensive permanent

10   marshes and swamps such as the Upemba wetland system (inundated area of 18,000 km^2) and the Luama swamps (inundated area of 6,000 km^2) (Hughes and Hughes 1992). Yet, it remains to be determined if the seasonality of CH_4 observed in Lualaba can be attributed to higher inputs during high water from these major wetlands located respectively, 1000 and 600 km upstream of Kisangani. Even so,

15   there are numerous more modest marshes and swamps that border upstream tributaries of the Lualaba closer to Kisangani (Hughes and Hughes 1992). The seasonal amplitude of dissolved CH_4 in the Oubangui was about 10 times higher than in the Kasaï and the Oubangui, and the seasonal amplitude of CH_4 in these three rivers seemed to be related to the relative seasonal amplitude of freshwater

20   discharge as indicated by the positive relation with the ratio of maximum and minimum of freshwater discharge (Fig. 22).

The seasonal cycles of %N_2O show patterns that were consistent with those CH_4, with a loose parallelism of %N_2O and discharge in the Lualaba, an inverse relation in the Kasaï, and peak of %N_2O during rising waters (although delayed with

25   respect to the CH_4 peak) in the Oubangui. In addition to the seasonal cycle there seemed to be a longer term decrease of the annual average of N_2O in the Lualaba (Fig. S13). There were no significant long term changes of the annual average of other variables such a POC, PN (not shown). So the observed decrease of annual N_2O is probably unrelated to changes in terrestrial productivity (Zhou et al. 2014) or

30   nitrogen content of terrestrial vegetation (Craine et al. 2018) that act at longer time scales (several decades) and seem to be related to long term changes in climate (precipitation). Freshwater discharge showed an increasing pattern during the time period (Fig. S13). An increasing discharge could lead to increased gas transfer velocities and a loss of N_2O to the atmosphere. Water temperature in the Congo

River is already close to the optimum of denitrification (~27°C, Canion et al. 2014), so an enhancement of denitrification with increase of temperature is unlikely. Water temperature did not show a clear pattern, but freshwater discharge increased during the 2013-2018 period, excluding the year 2017. It is likely that the decreasing trend in

5   N_2O during the 2013-2018 period is a transient feature in response to inter-annual fluctuations in hydrology that led to a period of sustained increase in freshwater discharge.

The pCO_2 time-series in the Lualaba at Kisangani is shorter than for CH_4, but a general positive relationship between pCO_2 and discharge was observed (Fig.

10   S14). A similar positive relationship between pCO_2 and discharge was also observed in the Oubangui (Bouillon et al. 2012) and the Madeira River (Almeida et al. 2017), as well in several rivers in the Amazon (Richey et al. 2002) based on pCO_2 calculated from pH and TA. Such pCO_2-discharge patterns were interpreted as resulting from higher connectivity during high-water between river mainstem and the floodplains

15   and wetlands. In large temperate rivers, a negative relationship between pCO_2 and discharge was observed in the Meuse (Borges et al. 2018) and in more than half of the US rivers analyzed by Liu and Raymond (2018). The difference in the relationship of pCO_2 versus discharge between tropical and temperate large rivers might be related to lower interactions between river and floodplains in temperate rivers in

20   particular in highly human-impacted and channelized rivers such as the Meuse. This is in agreement with the analysis of Aho and Raymond (2019) who reported, in the Salmon River network, positive relationships between pCO_2 and flow in water watersheds with a high presence of wetlands, and negative relationships between pCO_2 and flow in watersheds with low presence of wetlands. Also, in temperate

25   rivers, temperature co-varies strongly with discharge in temperate rivers, so that the warmer months that promote biological production of CO_2 are also characterized by lower discharge (Borges et al. 2018).

The seasonal amplitude of CH_4 (~50 nmol L^{-1} in the Kasaï and the Congo, versus 200-400 nmol L^{-1} in the Oubangui) and $\%N_2O$ (20-90% in the 3 rivers) was

30   overall much lower than the spatial gradients across the basin of 22 and 71,428 nmol L^{-1} for CH_4 and 0 and 561% for N_2O.

3.7.   Varibility of GHG fluxes in the Congo river network

Since pCO_2 and CH_4 and N_2O concentrations followed distinct patterns as a function of Strahler stream order (Fig. 11) we used k_{600} and stream surface area as a function of Strahler stream order (Fig. S15) to compute the air-water GHG fluxes and to integrate them at basin scale. This was done separating data for streams draining and not draining the CCC since pCO_2 and CH_4 and N_2O patterns were very different (Figs. 11 and 12). The stream surface area decreased regularly with increasing Strahler stream order but showed a large increase for Strahler stream order 9 (Fig. S15). The latter mainly corresponds to the Congo mainstem that downstream of Kisangani is characterized by anastomosing river channels with extended sand bars and numerous islands (Runge 2008; O'Loughlin et al. 2013). In particular along the section of about 500 km long between Mbandaka and Kwa mouth, the mainstem river channel undergoes a general expansion, and width increases from ~4 km to ~10 km. This corresponds to the area of CCC depression with a corresponding decrease of the slope from 6 to 3 cm km^{-1} (O'Loughlin et al. 2013). The calculated k_{600} decreased regularly with increasing Strahler stream order, as previously reported (Butman and Raymond 2011; Raymond et al. 2012; Deirmendjian and Abril 2018; Liu and Raymond 2018) due to higher turbulence in low order streams associated with higher stream flow due to steeper slopes. HydroSHEDS stream order classification is missing at least 1 stream order, because small streams are not correctly represented (Benstead and Leigh 2012; Raymond et al. 2013). Hence, to correct this bias, we added 1 to stream orders determined by HydroSHEDS, meaning that the lowest stream order to which GHG were attributed was 2. We then extrapolated pCO_2 and CH_4 and N_2O concentrations to stream order 1, separating streams draining and not draining the CCC, using a linear regression with higher orders or by using the same value as for order 2 (Fig. S16).

An error analysis on the GHG flux computation and upscaling was carried out by error propagation of the GHG concentration measurements, the k value estimates, and the estimate of surface areas of river channels to scale the areal fluxes, using a Monte Carlo simulation with 1000 iterations. The uncertainty on the GHG concentrations led to an uncertainty of areal fluxes of ±1.2%, ±2.3% and ±7.1% for CO_2, CH_4 and N_2O, respectively. The uncertainty on k derived from tracer experiments is typically ±30.0% (Ulseth et al. 2019). This leads to a cumulated uncertainty of areal fluxes of ±17.6%, ±17.9% and ±19.0% for CO_2, CH_4 and N_2O, respectively. The uncertainty of the river/stream surface areas based on GIS analysis

of Allen and and Pavelsky (2018) is estimated to ±10% leading to an overall uncertainty of integrated fluxes of ±18.3%, ±18.3% and ±19.6% for CO_2, CH_4 and N_2O, respectively.

The calculated FCO_2 ranged between 86 and 7,110 mmol m^{-2} d^{-1}, averaging 2,469±435 mmol m^{-2} d^{-1} (weighted by surface area of Strahler stream order), encompassing the range FCO_2 reported by Mann et al. (2014) (312 to 1,429 mmol m^{-2} d^{-1}) in 25 sites during a single period (November 2010) from four major river basins in the Republic of Congo (Alima, Lefini, Sangha, Likouala-Mossaka). The pCO_2 values ranged between 1,087 and 22,899 ppm, also encompassing the values reported by Mann et al. (2014) (2,600 to 15,802 ppm) that were not measured directly but computed from pH and DIC measurements, although pH measurements in black-water rivers can be biased by the presence of humic dissolved organic matter (Abril et al. 2015), and the addition of $HgCl_2$ seems to alter the CO_2 content of samples (Fig. S1). The calculated FCH_4 ranged between 65 and 597,260 µmol m^{-2} d^{-1}, averaging 12,553±2,247 µmol m^{-2} d^{-1} (weighted by surface area of Strahler order), encompassing the range FCH_4 reported by Upstill-Goddard et al. (2017) (33 to 48,705 µmol m^{-2} d^{-1}) in 41 sites draining the Congo basin in the Republic of Congo (November 2010 and August 2011) in the same four river basins sampled by Mann et al. (2014). The CH_4 values ranged between 22 and 71,428 nmol L^{-1}, also encompassing the values reported by Upstill-Goddard et al. (2017) (11 to 9,553 nmol L^{-1}). The calculated FN_2O ranged between -52 and 319 µmol m^{-2} d^{-1}, averaging 22±4 µmol m^{-2} d^{-1} (weighted by surface area of Strahler order), encompassing the range FN_2O reported by Upstill-Goddard et al. (2017) (-19 to 67 µmol m^{-2} d^{-1}). The $\%N_2O$ values ranged between 0 and 561 %, also encompassing the values reported by Upstill-Goddard et al. (2017) (6 to 266 %). The wider ranges of GHGs and respective fluxes we report compared to those of Mann et al. (2014) and Upstill-Goddard et al. (2017) reflect the larger number of river systems sampled over a wider geographical area (n=25 vs n=278 for pCO_2; n=41 vs n=367 for CH_4/N_2O), hence, representing a wider range of river types, morphologies, catchment characteristics, and wetland density.

Information on the seasonal variability of concurrent FCO_2, FCH_4 and FN_2O values was only available in the Lualaba (at Kisangani) where the three GHGs were measured simultaneously (Fig. S17). FCO_2, FCH_4 and FN_2O were loosely positively correlated with freshwater discharge, as the seasonal variations of k_{600} were small

(ranging between 23.4 and 30.3 cm h^{-1}), and although pCO$_2$ was correlated to freshwater discharge (Fig. S14) this was not the case for CH$_4$ and N$_2$O concentrations (Figs. 20 and 21). The range of seasonal variations at Kisangani of FCO$_2$ (234 and 948 mmol m^{-2} d^{-1}), FCH$_4$ (116 and 876 µmol m^{-2} d^{-1}) and FN$_2$O (-2 and 40 µmol m^{-2} d^{-1}) was small compared to the range of spatial variations of FCO$_2$ (86 and 7,110 mmol m^{-2} d^{-1}), FCH$_4$ (65 and 597,260 µmol m^{-2} d^{-1}), and FN$_2$O (-52 and 319 µmol m^{-2} d^{-1} µmol m^{-2} d^{-1}).

3.8. Significance of integrated GHG fluxes at basin and global scales

The FCO$_2$ and FCH$_4$ decreased with increasing Strahler order, as given by per surface area, and also when integrated by surface area of the streams (Table 1). Strahler orders 1-2 accounted for nearly 80% of the integrated FCO$_2$ (79.6%) and FCH$_4$ (77.0%), while Strahler orders 1-4 accounted for > 90% of the integrated FCO$_2$ (90.7%) and FCH$_4$ (91.9%). Strahler orders 5-10 only accounted for 9.3% of integrated FCO$_2$ and 8.1% of integrated FCH$_4$. The rivers draining the CCC contributed to 6% of the basin wide emissions for CO$_2$ and 22% for CH$_4$, although the contribution in stream surface area was only 11%. The low contribution of FCO$_2$ from the CCC to the basin wide emissions was due to the lower k_{600} values, although pCO$_2$ values were higher than the rest of the basin (Table 1). In the case of FCH$_4$, the much higher CH$_4$ concentrations in the CCC overcome the lower k_{600} values. FN$_2$O per surface area in rivers and streams outside the CCC were relatively similar for Strahler orders 10 to 3, and increased for Strahler orders 1 and 2 (Table 1). FN$_2$O per surface area in rivers and streams draining the CCC steadily decreased from Strahler order 8 to 1, with rivers of orders 5, 3, 2 and 1 acting as sinks for N$_2$O. Consequently, the relative contribution per Strahler order of integrated FN$_2$O was less skewed than for integrated FCO$_2$ and FCH$_4$. Strahler orders 1-4 contributed 69.9% of integrated FN$_2$O compared to >90% for FCO$_2$ and FCH$_4$.

The rivers and streams draining the CCC were a very small sink of atmospheric N$_2$O (-0.01 GgN$_2$O-N yr^{-1}) while the rivers and streams outside the CCC were a source of N$_2$O (5.1 GgN$_2$O-N yr^{-1}). The integrated FN$_2$O for the Congo River network was 5.1±1.0 GgN$_2$O-N yr^{-1} corresponded to 14-17% of total riverine emissions of N$_2$O reported by Hu et al. (2016). Note that the N$_2$O riverine emissions computed by Hu et al. (2016) were indirectly computed from data on global nitrogen

deposition on catchments and on emission factors rather than derived from direct measurements of dissolved N_2O concentrations. The estimates given by Hu et al. (2016) are more conservative than older estimates (e.g. Kroeze et al. 2010) because they are based on revised emission factors, and converge with a similar more recent

5   study by Maavara et al. (2018). Our estimate of the integrated FN_2O is consistent with the range of N_2O emissions of 3.8 to 4.3 GgN_2O-N yr^{-1} given by Maavara et al. (2018) for the Congo river network, also based on an indirect calculation based on nitrogen deposition and emission factors.

The integrated FCH_4 for the Congo River network of 1.7±0.3 $TgCH_4$ yr^{-1} is

10   nearly two times higher than the estimate given by Bastviken et al. (2011) for all tropical rivers, and corresponds to 6% of the global emission of CH_4 from rivers given by Stanley et al. (2016), while the surface area of Congo River network corresponds to a lower proportion (3 %) of the global riverine surface area (773,000 km^2, Allen and Pavelsky). Note that the meta-analysis of Stanley et al. (2016) includes part of

15   our data-set from Congo River, as published by Borges et al. (2015a). The integrated FCH_4 we report for the Congo River network is also more than three times higher than the estimate of CH_4 emissions for Amazonian large rivers reported by Sawakuchi et al. (2014) (0.49 $TgCH_4$ yr^{-1}). The integrated FCH_4 we report for the Congo River network corresponds to 7% of the emission from the Congo wetlands

20   inferred from remote sensed atmospheric CH_4 data (Bloom et al. 2010) (25.7 $TgCH_4$ yr^{-1}). However, the top-down estimate given by Bloom et al. (2011) includes the CH_4 emission from all ecosystems over the Congo basin, and should also include the fluvial emissions. Note that the CH_4 emissions we report for the Congo River basin only include the diffusive flux component, when the ebullitive CH_4 emission

25   component represents the majority of CH_4 emissions from inland waters (Bastviken et al. 2011), which would be consistent with the gap between our emission estimates and those from atmospheric CH_4 inventories. Finally, note that the CH_4 emissions were only calculated and integrated for the rivers and streams draining the CCC but not for the actual wetland flooded area of the CCC. The emission of CH_4 from actual

30   wetland flooded area of the CCC can be estimated to a massive 51 $TgCH_4$ yr^{-1} by extrapolating the area averaged FCH_4 from the streams (24,468 μmol m^{-2} d^{-1}, Table 1) to the flooded extent (360,000 km^2, Bwangoy et al. 2010). This corresponds to about 29% of the CH_4 emissions from natural wetlands (~180 $TgCH_4$ yr^{-1}, Saunois et al. 2010), and would in this case be higher than the estimate of CH_4 emissions from

the Congo wetlands inferred from remote sensed atmospheric CH_4 data (Bloom et al. 2010).

The integrated FCO_2 for the Congo River network is 251 ± 46 TgC yr^{-1} and is equivalent to the CO_2 emission value for rivers globally given by Cole et al. (2007), and to 14% and 39% of the CO_2 emission value for rivers globally given by Raymond et al. (2013) (1,8000 TgC yr^{-1}) and Lauerwald et al. (2015) (650 TgC yr^{-1}), respectively. The integrated CO_2 emission from the Congo River network corresponds to 44% of the CO_2 emissions from tropical (24°N-24°S) oceans globally (565 TgC yr^{-1}) and 183% of CO_2 emissions from the tropical Atlantic Ocean (137 TgC yr^{-1}), based on the Takahashi et al. (2002) FCO_2 climatology. The terrestrial net ecosystem exchange (NEE) of the watershed of the Congo River can be estimated based on the NEE estimate of 23 gC m^{-2} d^{-1} for savannahs given by Ciais et al. (2011) and of 20 gC m^{-2} d^{-1} for forests given by Fisher et al. (2013), and based on the respective land cover from GLC2009 (30% savannah and 70% forest). The corresponding terrestrial NEE of 77 TgC yr^{-1} is more than three times lower than the riverine CO_2 emission from the Congo River. This is extremely surprising since the hydrological export from *terra firme* forests of DOC and DIC, that are assumed to sustain fluvial emissions are typically 2-3% compared to terrestrial NEE (Kindler et al. 2011; Deirmendjian et al. 2018). Hydrological carbon export is higher compared to NEE in European grasslands (on average 22%) (Kindler et al. 2011). We ignore if this is transposable to tropical grasslands, such as savannahs, although they only occupy 30% of the Congo catchment surface. Accordingly, the CO_2 emission from the Congo River network should have been an order of magnitude lower than the estimates of terrestrial NEE from *terra firme* biomes rather than more than three times higher. However, in wetlands such as peatlands in Europe, the hydrological export of DOC and DIC represent 109% of NEE and is enough to sustain the riverine CO_2 emission that represents 17% of NEE (Billet et al. 2004). Indeed, the carbon export from flooded forests to riverine waters of the Congo basin can be roughly estimated to 396 TgC yr^{-1} and is in excess of the integrated FCO_2 (calculated from the export per surface area of flooded forest of 1,100 gC m^{-2} yr^{-1} reported by Abril et al. (2014) for the Central Amazon and on surface area of flooded forest of the CCC (360,000 km^{-2}, Bwangoy et al. 2010)). Altogether, this would then strongly suggest that the CO_2 emission from the lowland Congo River network is to a large extent sustained by another source of carbon than from the terrestrial *terra firme* biome. The

most likely alternative source would be wetlands (flooded forest and aquatic macrophytes), in agreement with the analysis in the Central Amazon River by Abril et al. (2013).

4. Conclusions

Net heterotrophy in rivers and lakes sustained by inputs of organic matter from the terrestrial vegetation on the catchments is the prevailing paradigm to explain over-saturation of CO_2 in inland surface waters and corresponding emissions to the
10   atmosphere, based on process studies, the earliest in the Amazon (Wissmar et al. 1981) and boreal systems (Del Giorgio et al. 1999; Prairie et al. 2002), and then generalised at global scales for lakes (Cole et al. 1994) and rivers (Cole and Caraco 2001). Yet, the comparison of 169 measurements of aquatic NEP and FCO_2 estimates in the central Congo River network covering a wide range of size and type
15   of rivers and streams shows that the aquatic NEP cannot account for fluvial FCO_2. This implies that lateral inputs of CO_2 sustain a large part of the CO_2 emissions from rivers and streams in the Congo River network.

The comparison of the integrated CO_2 emission from the Congo River network with terrestrial *terra firme* NEE shows that it unlikely that fluvial CO_2 emissions are
20   sustained by lateral hydrological transfer of carbon from *terra firme*. Indeed, integrated FCO_2 from the river network was more than three times higher than terrestrial NEE, when forests typically only export a very small fraction of NEE as carbon to rivers that can sustain fluvial CO_2 emissions. It is then likely that the fluvial CO_2 emissions from the central Congo River are sustained by organic matter inputs
25   as well as direct CO_2 inputs from extensive riparian wetlands (flooded forest and aquatic floating macrophytes). This is consistent with the stable isotopic signature of DIC, the differences in the spatial distribution of dissolved CO_2, $\%O_2$, and CH_4 between rivers and streams draining or not draining the CCC, a large wetland region in the core of the basin, and based on the correlation between pCO$_2$ levels and the
30   cover of flooded forest in the catchment. Indeed, the calculated export of carbon from the CCC to the riverine network is sufficient to sustain the the fluvial CO_2 emission from the Congo.

The fact that fluvial CO_2 emissions in lowland rivers are to a large extent sustained by carbon inputs from wetlands in addition to those from *terra firme* has

consequences for the conceptualisation of statistical and mechanistic models of carbon cycling in river networks. While progress has been made in integrating wetland connectivity in mechanistic regional models (Lauerwald et al. 2017), this has not been the case so far for statistical global models that rely on terrestrial (*terra firme*) productivity (Lauerwald et al. 2015). The comparison of the output of such a statistical model for the Congo River with observational data (Fig. S18) shows that the model fails to represent spatial gradients, and in particular the higher pCO_2 values of streams and rivers draining the CCC. This illustrates how ignoring the river-wetland connectivity can lead to the misrepresentation of pCO_2 dynamics in river networks, in particular tropical ones that account for the vast majority (80%) of global riverine CO_2 emissions.

Data availability. *Full data-set will be made publically available at www.zenodo.org should the manuscript be accepted in Biogeosciences.*

Author contributions. AVB and SB conceived the study; AVB, FD, TL, ET, ATS, TB, JB, CRT, SB collected field samples; AVB, FD, TL, CM, CRT, J-PD, SB made laboratory analysis; GA and TL carried out GIS analysis; AVB drafted the manuscript with substantial inputs from SB; all authors contributed to manuscript.

Acknowledgements. This work was funded by the European Research Council (ERC-StG 240002 AFRIVAL), the Fonds National de la Recherche Scientifique (FNRS, TransCongo, 14711103), the Belgian Federal Science Policy (BELSPO, COBAFISH SD/AR/05A), the Research Foundation Flanders (FWO-Vlaanderen), the Research Council of the KU Leuven, and the Fonds Leopold-III pour l'Exploration et Conservation de la Nature. The Boyekoli-Ebale-Congo 2010 Expedition was funded by the Belgian Development Cooperation, BELSPO, and Belgian National Lottery. We thank the Isotope Hydrology Laboratory of IAEA for analyses of water stable isotope ratios which contribute to the Coordinated Research Project CRPF33021 (Application and development of isotope techniques to evaluate human impacts on water balance and nutrient dynamics of large river basins) implemented by the IAEA, Jonathan Richir (University of Liège) for advise with the statistical analysis, Sandro Petrovic and Marc-Vincent Commarieu (University of Liège), Bruno Leporcq (UNamur), and Zita Kelemen (KU Leuven) for analytical assistance, the Régie des

Voies Fluviales (RFV, Kinshasa) for providing water height data, two anonymous reviewers for comments on the previous version of the manuscript. Publication costs were partly covered by European Geosciences Union as part of the 2018 Outstanding reviewer award to AVB. AVB is a senior research associate at the FNRS.

References

Abril, G., and Borges, A.V.: Carbon leaks from flooded land: do we need to re-plumb the inland water active pipe?, Biogeosciences, 16, 769-784, doi:10.5194/bg-16-769-2019, 2019.

Abril, G., Bouillon, S., Darchambeau, F., Teodoru, C. R., Marwick, T. R., Tamooh, F., Omengo, F. O., Geeraert, N., Deirmendjian, L., Polsenaere, P., and Borges A.V.: Technical note: Large overestimation of pCO_2 calculated from pH and alkalinity in acidic, organic-rich freshwaters, Biogeosciences, 12, 67-78, doi: 10.5194/bg-12-67-2015, 2015.

Abril, G., Martinez, J.-M., Artigas, L.F., Moreira-Turcq, P., Benedetti, M.F., Vidal, L., Meziane, T., Kim, J.-H., Bernardes, M.C., Savoye, N., Deborde, J., Albéric, P., Souza, M.F.L., Souza, E.L., and Roland, F.: Amazon river carbon dioxide outgassing fuelled by wetlands, Nature, 505, 395-398, doi: 10.1038/nature12797, 2014.

Allen, G. H., and Pavelsky, T. M.: Global extent of rivers and streams, Science, 28, eaat0636, doi: 10.1126/science.aat0636, 2018.

Almeida, R. M. , Pacheco, F. S., Barros, N., Rosi, E., and Roland, F.: Extreme floods increase CO_2 outgassing from a large Amazonian river, Limnol. Oceanogr. , 62, 989-999, doi: 10.1002/lno.10480, 2017.

Alsdorf, D., Beighley, E., Laraque, A., Lee, H., Tshimanga, R., O'Loughlin, F., Mahé, G., Dinga, B., Moukandi, G., and Spencer, R. G. M. : Opportunities for hydrologic research in the Congo Basin, Rev. Geophys., 54, 378-409, doi: 10.1002/2016RG000517, 2016.

Amaral, J. H. F., Borges, A. V., Melack, J. M., Sarmento, H., Barbosa, P. M., Kasper, D., Melo, M. L., de Fex Wolf, D., da Silva, J. S., and Forsberg, B. R.: Influence of plankton metabolism and mixing depth on CO_2 dynamics in an Amazon floodplain lake, Sci. Total Environ., 630, 1381-1393, doi: 10.1016/j.scitotenv.2018.02.331, 2018.

APHA, Standard methods for the examination of water and wastewater, American Public Health Association. 1998.

Balagizi, C. M., Darchambeau, F., Bouillon, S., Yalire, M.M., Lambert, T., and Borges, A. V.: River geochemistry, chemical weathering and atmospheric CO_2 consumption rates in the Virunga Volcanic Province (East Africa), Geochem. Geophys. Geosys., 16, doi:10.1002/2015GC005999, 2015.

Barbosa, P.M., Melack, J.M., Farjalla, V. F., Amaral, J. H. F., Scofield, V., and Forsberg, B. R.: Diffusive methane fluxes from Negro, Solimões and Madeira rivers and fringing lakes in the Amazon basin, Limnol. Oceanogr., 61, S221-S237, doi: 10.1002/lno.10358, 2016.

Bastviken, D., Ejlertsson, J., and Tranvik, L.: Measurement of methane oxidation in lakes: A comparison of methods. Environ. Sci. Technol. 36, 3354-3361, doi: 10.1021/es010311p, 2002.

Bastviken, D., Tranvik, L. J., Downing, J. A., Crill, P. M., and Enrich-Prast, A. :, Freshwater methane emissions offset the continental carbon sink, Science, 331, 50, doi: 10.1126/science.1196808, 2011.

Battin, T. J., Kaplan, L. A., Findlay, S., Hopkinson, C. S., Marti, E., Packman, A. I., Newbold, J. D, and Sabater, F : Biophysical controls on organic carbon fluxes in fluvial networks, Nat. Geosci., 1, 95-100, doi: 10.1038/ngeo101, 2008.

Baulch, H. M., Schiff, S. L., Maranger, R., and Dillon, P. J.: Nitrogen enrichment and the emission of nitrous oxide from streams, Global Biogeochem. Cycles, 25, GB4013, doi:10.1029/2011GB004047, 2011.

Benstead, J. P., and Leigh, D. S.: An expanded role for river networks. Nature Geosci. 5, 678-679 536, doi: 10.1038/ngeo1593, 2012.

Billett, M. F., Palmer, S. M., Hope, D., Deacon, C., Storeton-West, R., Hargreaves, K. J., Flechard, C., and Fowler, D.: Linking land-atmosphere-stream carbon fluxes in a lowland peatland system, Global Biogeochem. Cycles, 18, GB1024, doi:10.1029/2003GB002058, 2004.

Bird, M. I., Giresse, P., and Chivas, A. R.: Effect of forest and savanna vegetation on the carbon-isotope composition from the Sanaga River, Cameroon. Limnol. Oceanogr., 39,1845-54, doi:10.4319/lo.1994.39.8.1845, 1994.

Bird, M. I., and Pousai, P.: Variations of $\delta^{13}C$ in the surface soil organic carbon pool. Global Biogeoch. Cycles, 11, 313-322, doi: 10.1029/97GB01197, 1997.

Deirmendjian, L., and Abril, G.: Carbon dioxide degassing at the groundwater-stream-atmosphere interface: isotopic equilibration and hydrological mass balance in a sandy watershed, J. Hydrol 558, 129-143, doi:10.1016/j.jhydrol.2018.01.0030022-1694, 2018.

Bloom, A. A., Palmer, P. I., Fraser, A., Reay, D. S., Frankenberg, C.: Large-scale controls of methanogenesis inferred from methane and gravity spaceborne data. Science, 327, 322-325, doi: 10.1126/science.1175176, 2010.

Borges, A. V., Darchambeau, F., Lambert, T., Bouillon, S., Morana, C., Brouyère, S., Hakoun, V., Jurado, A., Tseng, H.-C., Descy, J.-P., Roland, F. A. E.: Effects of agricultural land use on fluvial carbon dioxide, methane and nitrous oxide concentrations in a large European river, the Meuse (Belgium). Sci. Total Environ., 610-611, 342-355, doi: 10.1016/j.scitotenv.2017.08.047, 2018.

Borges, A. V., Darchambeau, F., Teodoru, C. R., Marwick, T. R., Tamooh, F., Geeraert, N., Omengo, F. O., Guérin, F., Lambert, T., Morana, C., Okuku, E., and Bouillon, S.: Globally significant greenhouse gas emissions from African inland waters, Nature Geosci., 8, 637-642, doi:10.1038/NGEO2486, 2015a.

Borges, A. V., Abril, G., Darchambeau, F., Teodoru, C. R., Deborde, J., Vidal, L. O., Lambert, T., and Bouillon, S.: Divergent biophysical controls of aquatic CO2 and CH4 in the World's two largest rivers, Sci. Rep., 5, 15614, doi: 10.1038/srep15614, 2015b.

Bouillon, S., Yambélé, A., Gillikin, D. P., Teodoru, C., Darchambeau, F., Lambert, T., and Borges, A.V.: Contrasting biogeochemical characteristics of right-bank tributaries and a comparison with the mainstem Oubangui River, Central African Republic (Congo River basin), Sci. Rep., 4, 5402, doi: 10.1038/srep05402, 2014.

Bouillon, S., Yambélé, A., Spencer, R. G. M., Gillikin, D. P., Hernes, P. J., Six, J., Merckx, R., and Borges A. V.: Organic matter sources, fluxes and greenhouse gas exchange in the Oubangui River (Congo River basin), Biogeosciences, 9, 2045-2062, 2012.

Bouillon, S., Abril, G., Borges, A. V., Dehairs, F., Govers, G., Hughes, H. J., Merckx, R., Meysman, F. J. R., Nyunja, J., Osburn, C., and Middelburg, J. J.: Distribution, origin and cycling of carbon in the Tana River (Kenya): a dry season basin-scale survey from headwaters to the delta, Biogeosciences, 6, 2475–2493, doi:10.5194/bg-6-2475-2009, 2009.

Bultot, F. : Atlas Climatique du Bassin Congolais Publications de L'Institut National pour L'Etude Agronomique du Congo (I.N.E.A.C.), Troisieme Partie, Temperature et Humidite de L'Air, Rosee, Temperature du Sol, 1972.

Butman, D., and Raymond, P. A.: Significant efflux of carbon dioxide from streams and rivers in the United States. Nature Geosci., 4, 839-842, doi: 10.1038/NGEO1294, 2011.

Bwangoy, J.-R. B., Hansen, M. C., Roy, D. P., De Grandi, G., and Justice, C. O.: Wetland mapping in the Congo Basin using optical and radar remotely sensed data and derived topographical indices, Remote Sens. Environ., 114, 73-86, doi:10.1016/j.rse.2009.08.004, 2010.

Canion, A., Overholt, W. A., Kostka, J. E., Huettel, M., Lavik, G., and Kuypers, M. M. M.: Temperature response of denitrification and anaerobic ammonium oxidation rates and microbial community structure in Arctic fjord sediments, Environ. Microbiol., 16, 3331-3344, doi:10.1111/1462-2920.12593, 2014.

Cardoso, S. J., Enrich-Prast, A., Pace, M. L., and Roland, F.: Do models of organic carbon mineralization extrapolate to warmer tropical sediments? Limnol. Oceanogr., 59, 48-54, doi:10.4319/lo.2014.59.1.0048, 2014.

Ciais, P., Bombelli, A., Williams, M., Piao, S. L., Chave, J., Ryan, C. M., Henry, M., Brender, P., and Valentini, R.: The carbon balance of Africa: synthesis of recent research studies. Phil. Trans. R. Soc. A, 369, 2038-2057, doi: 10.1098/rsta.2010.0328, 2013.

Coplen, T. B., and Wassenaar, L. I.: LIMS for Lasers 2015 for achieving long-term accuracy and precision of δ^2H, δ^{17}O, and δ^{18}O of waters using laser absorption spectrometry, Rapid comm. mass spectrum., 29, 2122-2130, doi: 10.1002/rcm.7372,2015.

Cole, B. E., and Cloern, J. E.: An empirical model for estimating phytoplankton productivity in estuaries. Mar. Ecol. Prog. Ser., 36, 299-305, doi: 10.3354/meps036299, 1987.

Cole, J. J., and Caraco, N. F.: Carbon in catchments: connecting terrestrial carbon losses with aquatic metabolism. Mar. Fresh. Res., 52, 101-110, doi: 10.1071/MF00084, 2001.

Cole, J. J., Caraco, N. F., Kling, G. W., and Kratz, T. K.: Carbon dioxide supersaturation in the surface waters of lakes. Science, 265, 1568-1570, doi: 10.1126/science.265.5178.1568, 1994.

Cole, J. J., Prairie, Y. T., Caraco, N. F., McDowell, W. H., Tranvik, L. J., Striegl, R. G. , Duarte, C. M., Kortelainen, P., Downing, J. A., Middelburg, J. J., and Melack, J.: Plumbing the global carbon cycle: Integrating inland waters into the terrestrial carbon budget. Ecosystems, 10, 171-184, doi:10.1007/s10021-006-9013-8, 2007.

Coynel, A., Seyler, P., Etcheber, H., Meybeck, M., and Orange, D.: Spatial and seasonal dynamics of total suspended sediment and organic carbon species in the Congo River, Global Biogeochem. Cycles, 19, GB4019, doi:10.1029/2004GB002335, 2005.

Craine J. M., Elmore, A. J., Wang, L., Aranibar, J., Bauters, M., Boeckx, P., Crowley, B. E., Dawes, M. A., Delzon, S., Fajardo, A., Fang, Y., Fujiyoshi, L., Gray, A.,

Guerrieri, R., Gundale, M. J., Hawke, D.J., Hietz, P., Jonard, M., Kearsley, E., Kenzo, T., Makarov, M., Marañón-Jiménez, S., McGlynn, T. P., McNeil, B. E., Mosher, S. G., Nelson, D. M., Peri, P. L., Roggy, J. C., Sanders-DeMott, R., Song, M., Szpak, P., Templer, P. H., Van der Colff, D., Werner, C., Xu, X., Yang, Y., Yu, G., and Zmudczyńska-Skarbek K.: Isotopic evidence for oligotrophication of terrestrial ecosystems, Nat. Ecol. Evol., 2, 1735-1744, doi:10.1038/s41559-018-0694-0, 2018.

Crawford J. T., Stanley, E. H., Dornblaser, M., Striegl, R. G.: CO_2 time series patterns in contrasting headwater streams of North America, Aquat. Sci., 79, 473-486, doi:10.1007/s00027-016-0511-2, 2017.

Dargie, G. C., Lewis, S. L., Lawson, I. T., Mitchard, E. T. A., Page, S. E., Bocko, Y. E., and Ifo, S. A.: Age, extent and carbon storage of the central Congo Basin peatland complex, Nature, 542, 86-90, 10.1038/nature21048, 2017.

Deirmendjian, L., Loustau, D., Augusto, L., Lafont, S., Chipeaux, C., Poirier, D., and Abril, G.: Hydro-ecological controls on dissolved carbon dynamics in groundwater and export to streams in a temperate pine forest. Biogeosciences, 15, 669-691, doi:10.5194/bg-15-669-2018, 2018.

Deirmendjian, L., and Abril, G.: Carbon dioxide degassing at the groundwater-stream-atmosphere interface: isotopic equilibration and hydrological mass balance in a sandy watershed, J. Hydrol., 558, 129–143, doi:, 10.1016/j.jhydrol.2018.01.0030022-1694, 2018.

Dinsmore, K. J., Wallin, M. B., Johnson, M. S., Billett, M. F., Bishop, K., Pumpanen, J., Ojala, A.: Contrasting CO_2 concentration discharge dynamics in headwater streams: a multi-catchment comparison. J. Geophys. Res., 118, 445-461, doi:10.1002/jgrg.20047 ,2013.

Del Giorgio, P. A., Cole, J. J., Caraco, N. F., and Peters, R. H.: Linking planktonic biomass and metabolism to net gas fluxes in northern temperate lakes. Ecology, 80, 1422-1431, doi: 10.1890/0012-9658(1999)080[1422:LPBAMT]2.0.CO;2, 1999.

Descy, J.-P., Hardy, M.-A., Sténuite, S., Pirlot, S., Leporcq, B., Kimirei, I., Sekadende, B., Mwaitega, S. R., and Sinyenza, D.: Phytoplankton pigments and community composition in Lake Tanganyika. Freshwater Biology, 50, 668-684, doi: 10.1111/j.1365-2427.2005.01358.x, 2005.

Descy, J.-P., Darchambeau, F., Lambert, T., Stoyneva, M. P., Bouillon, S., and Borges, A. V.: Phytoplankton dynamics in the Congo River. Freshw. Biol., 62, 87-101, doi:10.1111/fwb.12851, 2017.

Doctor, D. H., Kendall, C., Sebestyen, S. D., Shanley, J. B., Ohte, N., and Boyer, E. W.: Carbon isotope fractionation of dissolved inorganic carbon (DIC) due to outgassing of carbon dioxide from a headwater stream, Hydrol. Process., 22, 2410-2423, doi: 10.1002/hyp.6833, 2008.

Downing, J. A., Cole, J. J., Duarte, C. M., Middelburg, J. J., Melack, J. M., Prairie, Y. T., Kortelainen, P., Striegl, R. G., McDowell, W. H., and Tranvik, L. J.: Global abundance and size distribution of streams and rivers. Inland Waters, 2, 229-236, doi:10.5268/IW-2.4.502, 2012.

Duvert, C., Butman, D.E., Marx, A., Ribolzi, O., and Hutley, L.B.: CO_2 evasion along streams driven by groundwater inputs and geomorphic controls, Nature Geosci., 11, 813–818, doi:10.1038/s41561-018-0245-y, 2018.

Fisher, J. B., Sikka, M., Sitch, S., Ciais, P., Poulter, B., Galbraith, D., Lee, J.-E., Huntingford, C., Viovy, N., Zeng, N., Ahlström, A., Lomas, M. R., Levy, P. E., Frankenberg, C., Saatchi, S., and Malhi, Y.: African tropical rainforest net

carbon dioxide fluxes in the twentieth century. Phil. Trans. R. Soc. B, 368, 20120376, doi:10.1098/rstb.2012.0376, 2013.

Fluet-Chouinard, E., Lehner, B., Rebelo, L.-M., Papa, F., and Hamilton, S.K.: Development of a global inundation map at high spatial resolution from topographic downscaling of coarse-scale remote sensing data. Remote Sens. Environ., 158, 348-361, doi:10.1016/j.rse.2014.10.015, 2015.

Frankignoulle, M., Borges, A., and Biondo R.: A new design of equilibrator to monitor carbon dioxide in highly dynamic and turbid environments. Water Res., 35, 1344-1347, doi:10.1016/S0043-1354(00)00369-9, 2001.

Gaillardet, J., Dupré, B., Louvat, P., and Allègre C. J.: Global silicate weathering and CO_2 consumption rates deduced from the chemistry of large rivers, Chem. Geol., 159, 3-30, doi: 10.1016/S0009-2541(99)00031-5, 1999.

Gillikin, D.P., and Bouillon, S.: Determination of $\delta^{18}O$ of water and $\delta^{13}C$ of dissolved inorganic carbon using a simple modification of an elemental analyzer – isotope ratio mass spectrometer (EA-IRMS): an evaluation, Rapid Comm. Mass Spectrom., 21, 1475-1478, doi: 10.1002/rcm.2968, 2007.

Gran, G.: Determination of the equivalence point in potentiometric titrations Part II, The Analyst, 77, 661-671, doi:10.1039/AN9527700661, 1952.

Hamilton, S. K., Sippel, S. J., and Melack J. M.: Comparison of inundation patterns among major South American floodplains, J. Geophys. Res., 107, LBA 5-1-LBA 5-14, doi: 10.1029/2000JD000306, 2002.

Happell, J., Chanton, J.P., and Showers, W.: The influence of methane oxidation on the stable isotopic composition of methane emitted from Florida Swamp forests. Geochim. Cosmochim. Acta, 58, 4377-4388, doi:10.1016/0016-7037(94)90341-7, 1994.

Hedges, J. I., Clark, W. A., Quay, P. D., Richey, J. E., Devol, A. H., and de M. Santos U.: Compositions and fluxes of particulate organic material in the Amazon River. Limnol Oceanogr., 31, 717-738, doi: 10.4319/lo.1986.31.4.0717, 1986.

Hotchkiss, E. R., Hall Jr, R. O., Sponseller, R. A., Butman, D., Klaminder, J., Laudon, H., Rosvall, M., and Karlsson, J.: Sources of and processes controlling CO2 emissions change with the size of streams and rivers, Nature Geosci., 8, 696-699, doi:10.1038/ngeo2507, 2015.

Hu, M., Chen, D., and Dahlgren, R. A.: Modeling nitrous oxide emission from rivers: a global Assessment, Glob. Change Biol., 22, 3566-3582, doi: 10.1111/gcb.13351, 2016.

Hughes, R. H., and Hughes, J. S.: A directory of African wetlands. IUCN. ISBN 2-88032-949-3, 1992.

Huotari, J., Haapanala, S., Pumpanen, J., Vesala, T., and Ojala, A.: Efficient gas exchange between a boreal river and the atmosphere, Geophys. Res. Lett., 40, 5683–5686, doi:10.1002/2013GL057705, 2013.

Kindler, R., Siemens, J., Kaiser, K., Walmsley, D. C., Bernhofer, C., Buchmann, N., Cellier, P., Eugster, W., Gleixner, G., Grunwald, T., Heim, A., Ibrom, A., Jones, S. K., Jones, M., Klumpp, K., Kutsch, W., Steenberg Larsen, K., Lehuger, S., Loubet, B., McKenzie, R., Moors, E., Osborne, B., Pilegaard, K., Rebmann, C., Saunders, M., Schmidt, M. W. I., Schrumpf, M., Seyfferth, J., Skiba, U., Soussana, J.-F., Sutton, M. A.; Tefs, C., Vowinckel, B., Zeeman, M. J., and Kaupenjohann, M.: Dissolved carbon leaching from soil is a crucial component of net ecosystem carbon balance. Glob. Change Biol., 17, 1167–1185, doi: 10.1111/j.1365-2486.2010.02282.x, 2011.

Klaus, M., Geibrink, E., Jonsson, A., Bergström, A.-K., Bastviken, D., Laudon, H., Klaminder, J., Karlsson, J.: Greenhouse gas emissions from boreal inland waters unchanged after forest harvesting. Biogeosciences, 15, 5575-5594, doi: 10.5194/bg-15-5575-2018, 2018.

5 Kokic, J., Sahlée, E., Sobek, S., Vachon, D., Wallin, M. B.: High spatial variability of gas transfer velocity in streams revealed by turbulence measurements. Inland Waters, doi:10.1080/20442041.2018.1500228, 2018.

Koné, Y. J. M., Abril, G., Delille, B., and Borges, A.V.: Seasonal variability of methane in the rivers and lagoons of Ivory Coast (West Africa), Biogeochemistry, 100, 21-37, doi: 10.1007/s10533-009-9402-0, 2010.

Koné Y. J. M., Abril, G., Kouadio, K.N., Delille, B., and Borges, A. V.: Seasonal variability of carbon dioxide in the rivers and lagoons of Ivory Coast (West Africa), Estuar. Coast., 32, 246-260, doi: 10.1007/s12237-008-9121-0, 2009.

Kosten, S., Piñeiro, M., de Goede, E., de Klein, J., Lamers, L. P. M., Ettwig, K.: Fate of methane in aquatic systems dominated by free-floating plants, Water Res., 104, 200-207, doi:j.watres.2016.07.054, 2016.

Kroeze, C., Dumont, E., Seitzinger, S. P.: Future trends in emissions of N_2O from rivers and estuaries. J. Integr. Environ. Sc., 7, 71–78, doi: 10.1080/1943815X.2010.496789, 2010.

20 Lambert, T., Bouillon, S., Darchambeau, F., Massicotte, P., and Borges, A.V.: Shift in the chemical composition of dissolved organic matter in the Congo River network, Biogeosciences, 13, 5405–5420, 2016, doi:10.5194/bg-13-5405-2016, 2016.

Laraque, A., Mietton, M. Olivry, J. C., Pandi, A.: Impact of lithological and vegetal covers on flow discharge and water quality of Congolese tributaries from the Congo river. Rev. Sci. Eau , 11, 209-224, doi:10.7202/705304a, 1998.

Laraque, A., Bricquet, J.P., Pandi, A., and Olivry, J.C.: A review of material transport by the Congo River and its tributaries. Hydrol. Process., 23, 3216-3224, doi: 10.1002/hyp.7395, 2009.

30 Lauerwald, R., Regnier, P., Camino-Serrano, M., Guenet, B., Guimberteau, M., Ducharne, A., Polcher, J., and Ciais P.: ORCHILEAK (revision 3875): a new model branch to simulate carbon transfers along the terrestrial–aquatic continuum of the Amazon basin. Geosci. Model Dev., 10, 3821-3859, doi:10.5194/gmd-10-3821-2017, 2017.

35 Lauerwald, R., Laruelle, G. G., Hartmann, J., Ciais, P., and Regnier, P. A. G.: Spatial patterns in CO_2 evasion from the global river network, Global Biogeochem. Cycles, 29, 534-554, doi:10.1002/2014GB004941, 2015.

Le, T. T. H., Fettig, J., and Meon, G.: Kinetics and simulation of nitrification at various pH values of a polluted river in the tropics, Ecohydrol. Hydrobiol., 19, 54-65, 2019.

40 Liptay, K., Chanton, J., Czepiel, P., and Mosher, B.: Use of stable isotopes to determine methane oxidation in landfill cover soils. J. Geophys. Res., 103, 8243-8250, doi: 10.1029/97JD02630, 1998.

Liss, P. S., Slater, P. G.: Flux of gases across the air sea interface. Nature, 247, 181-184, doi:10.1038/247181a0, 1974.

45 Liu, S., and Raymond, P. A.: Hydrologic controls on pCO_2 and CO_2 efflux in US streams and rivers, Limnol. Oceanogr. Lett., 3, 428-435, doi: 10.1002/lol2.10095, 2018.

Lynch, J. K., Beatty, C. M., Seidel, M. P., Jungst, L. J., DeGrandpre, M. D.: Controls
50 of riverine CO_2 over an annual cycle determined using direct, high temporal

resolution pCO_2 measurements. J. Geophys. Res., 115, G03016, doi:10.1029/2009JG001132, 2010.

Maavara, T., Lauerwald, R., Laruelle, G.G., Akbarzadeh, Z., Bouskill, N. J., Van Cappellen, P., and Regnier, P.: Nitrous oxide emissions from inland waters: Are IPCC estimates too high? Glob. Change Biol., 10.1111/gcb.14504, 2018.

Malhi, Y., Adu-Bredu, S., Asare, R. A., Lewis, S. L., and Mayaux, P.: African rainforests: past, present and future. Phil. Trans. R. Soc. B, 368: 20120312, doi:10.1098/rstb.2012.0312, 2013.

Mann, P. J., Spencer, R. G. M., Dinga, B. J., Poulsen, J. R., Hernes, P. J., Fiske, G., Salter, M. E., Wang, Z. A., Hoering, K. A., Six, J., and Holmes R. M.: The biogeochemistry of carbon across a gradient of streams and rivers within the Congo Basin. J. Geophys. Res. Biogeosci., 119, 687-702, 10.1002/2013JG002442, 2014.

Maurice, L., Rawlins, B. G., Farr, G., Bell, R., and Gooddy, D. C.: The influence of flow and bed slope on gas transfer in steep streams and their implications for evasion of CO2. J. Geophys. Res.: Biogeosciences, 122, 2862-2875, doi:10.1002/2017JG004045, 2017.

Marwick, T. R., Tamooh, F., Ogwoka, B., Teodoru, C., Borges, A. V., Darchambeau, F., and Bouillon, S.: Dynamic seasonal nitrogen cycling in response to anthropogenic N loading in a tropical catchment, Athi–Galana–Sabaki River, Kenya, Biogeosciences, 11, 1-18, doi:10.5194/bg-11-1-2014, 2014.

Marx, A., Dusek, J., Jankovec, J., Sanda, M., Vogel, T., van Geldern, R., Hartmann, J., and Barth, J. A. C.: A review of CO_2 and associated carbon dynamics in headwater streams: A global perspective, Rev. Geophys., 55, 560–585, doi:10.1002/2016RG000547, 2017.

McDowell, M. J., and Johnson, M. S.: Gas transfer velocities evaluated using carbon dioxide as a tracer show high streamflow to be a major driver of total CO_2 evasion flux for a headwater stream. J. Geophys. Res.: Biogeosciences, 123, 2183-2197. doi:10.1029/2018JG004388, 2018.

Melack, J. M., Hess, L. L., Gastil, M., Forsberg, B. R., Hamilton, S. K., Lima, I. B. T., Novo, E. M. L. M.: Regionalization of methane emissions in the Amazon Basin with microwave remote sensing. Glob. Change Biol. 10, 530-544, doi:10.1111/j.1365-2486.2004.00763.x, 2004.

Meybeck, M.: Global chemical weathering of surficial rocks estimated from river dissolved loads. Am. J. Sci. 287, 401-428, doi: 10.2475/ajs.287.5.401, 1987.

Millero, F. J.: The thermodynamics of the carbonate system in seawater. Geochem. Cosmochem. Acta, 43, 1651-1661, doi: 10.1016/0016-7037(79)90184-4,1979.

Morana, C., Borges, A. V., Roland, F. A. E., Darchambeau, F., Descy, J.-P., and Bouillon, S.: Methanotrophy within the water column of a large meromictic, tropical lake (Lake Kivu, East Africa). Biogeosciences, 12, 2077-2088, doi:10.5194/bg-12-2077-2015, 2015.

Nkounkou, R.R., and Probst, J.L. : Hydrology and geochemistry of the Congo river system. Mitt. Geol–Palaont. Inst. Univ. Hamburg, SCOPE/UNEP, 64, 483-508, 1987.

O'Loughlin, F., Trigg, M. A., Schumann, G. J.-P., and Bates, P. D.: Hydraulic characterization of the middle reach of the Congo River, Water Resour. Res., 49, 5059-5070, doi:10.1002/wrcr.20398, 2013.

Peter, H., Singer, G. A., Preiler, C., Chifflard, P., Steniczka, G., Battin, T. J.: Scales and drivers of temporal pCO_2 dynamics in an Alpine stream. J. Geophys. Res. Biogeosci., 119, 1078-1091, doi:10.1002/2013JG002552, 2014.

Powell, R.L., Yoo, E.-H., and Still, C.J.: Vegetation and soil carbon-13 isoscapes for South America: integrating remote sensing and ecosystem isotope measurements. Ecosphere 3, 1-25, doi: 10.1890/ES12-00162.1,2012.

Prairie, Y. T., Bird, D. F., Cole, J. J.: The summer metabolic balance in the epilimnion of southeastern Quebec lakes. Limnol. Oceanogr., 47, 316-321, 10.4319/lo.2002.47.1.0316, 2002.

Raymond, P. A., Hartmann, J., Lauerwald, R., Sobek, S., McDonald, C., Hoover, M., Butman, D., Striegl, R., Mayorga, E., Humborg, C., Kortelainen, P., Dürr, H., Meybeck, M., Ciais, P., and Guth, P.: Global carbon dioxide emissions from inland waters, Nature, 503, 355-359, 10.1038/nature12760, 2013.

Raymond, P. A., Zappa, C. J., Butman, D., Bott, T. L., Potter, C., Mulholland, P., Laursen, A. E., McDowell, W. H., and Newbold, D.: Scaling the gas transfer velocity and hydraulic geometry in streams and small rivers. Limnol. Oceanogr. Fluids Environ., 2, 41-53, doi: 10.1215/21573689-1597669, 2012.

Reiman, J. H., Xu, J. Y.: Diel variability of pCO_2 and CO_2 outgassing from the Lower Mississippi River: Implications for riverine CO_2 outgassing estimation, Water, 11, 43, 1-15, doi:10.3390/w11010043, 2019.

Richardson, D. C., Newbold, J. D., Aufdenkampe, A. K., Taylor, P. G., and Kaplan, L. A.: Measuring heterotrophic respiration rates of suspended particulate organic carbon from stream ecosystems, Limnol. Oceanogr.: Methods 11, 247-261, doi:10.4319/lom.2013.11.247, 2013.

Richey, J. E., Devol, A. H., Wofy, S. C., Victoria, R., and Riberio, M. N. G.: Biogenic gases and the oxidation and reduction of carbon in Amazon River and floodplain waters. Limnol. Oceanogr., 33, 551-561, doi:10.4319/lo.1988.33.4.0551, 1988.

Richey, J. E., Melack, J. M., Aufdenkampe, A. K., Ballester, V. M., Hess, L.: Outgassing from Amazonian rivers and wetlands as a large tropical source of atmospheric CO_2. Nature, 416, 617-620, doi:10.1038/416617a, 2002.

Runge, J.: in Large Rivers: Geomorpholgy and Management (ed Gupta, A.), 293-309, John Wiley & Sons. 2008.

Santos, I.R., Maher, D.T., and, Eyre B.D.: Coupling automated radon and carbon dioxide measurements in coastal waters, Environ. Sci. Technol. 46, 7685-7691, doi:10.1021/es301961b, 2012.

Sawakuchi, H. O., Bastviken, D., A.O. Sawakuchi, N.D. Ward, C.D. Borges, S.M. Tsai, J.E . Richey, M.V.R. Ballester and A.V. Krusche, Oxidative mitigation of aquatic methane emissions in large Amazonian rivers, Global Change Biology (2016) 22, 1075–1085, doi: 10.1111/gcb.13169

Sawakuchi, H. O., Bastviken, D., Sawakuchi, A. O., Krusche, A. V., Ballester, M. V. R., and Richey, J.E.: Methane emissions from Amazonian Rivers and their contribution to the global methane budget, Glob. Change Biol., 20, 2829-2840, doi: 10.1111/gcb.12646, 2014.

Saunois, M., Bousquet, P., Poulter, B., Peregon, A., Ciais, P., Canadell, J. G., Dlugokencky, E. J., Etiope, G., Bastviken, D., Houweling, S., Janssens-Maenhout, G., Tubiello, F. N., Castaldi, S., Jackson, R. B., Alexe, M., Arora, V. K., Beerling, D. J., Bergamaschi, P., Blake, D. R., Brailsford, G., Brovkin, V., Bruhwiler, L., Crevoisier, C., Crill, P., Kovey, K., Curry, C., Frankenberg, C., Gedney, N., Höglund-Isaksson, L., Ishizawa, M., Ito, A., Joos, F., Kim, H.-S., Kleinen, T., Krummel, P., Lamarque, J.-F., Langenfelds, R., Locatelli, R., Machida, T., Maksyutov, S., McDonald, K. C., Marshall, J., Melton, J. R., Morino, I., Naik, V., O'Doherty, S., Parmentier, F.-J. W., Patra, P. K., Peng, C.,

Peng, S., Peters, G., Pison, I., Prigent, C., Prinn, R., Ramonet, M., Riley, W. J., Saito, M., Sanyini, M., Schroeder, R., Simpson, I. J., Spahni, R., Steele, P., Takizawa, A., Thornton, B. F., Tian, H., Tohjima, Y., Viovy, N., Voulgarakis, A., van Weele, M., van der Werf, G., Weiss, R., Wiedinmyer, C., Wilton, D. J., Wiltshire, A., Worthy, D., Wunch, D. B., Xu, X., Yoshida, Y., Zhang, B., Zhang, Z., Zhu, Q.: The global methane budget, Earth System Science Data, 8, 697-751, doi: 10.5194/essd-8-697-2016, 2016.

Scofield, V., Melack, J. M., Barbosa, P. M., Amaral, J. H. F., Forsberg, B. R., and Farjalla, V. F.: Carbon dioxide outgassing from Amazonian aquatic ecosystems in the Negro River basin, Biogeochemistry, 129, 77-91, doi: 10.1007/s10533-016-0220-x, 2016.

Seitzinger, S. P., Kroeze, C.: Global distribution of nitrous oxide production and N inputs in freshwater and coastal marine ecosystems. Global Biogeochem. Cycles, 12, 93-113, doi:10.1029/97GB03657, 1998.

Simpson, H., and Herczeg, A.: Stable isotopes as an indicator of evaporation in the River Murray, Australia, Water Resour. Res., 27, 1925-1935, doi:10.1029/91WR00941, 1991.

Spencer, R. G. M., Hernes, P. J., Aufdenkampe, A. K., Baker, A., Gulliver, P., Stubbins, A., Aiken, G. R., Dyda, R. Y., Butler, K. D., Mwamba, V. L., Mangangu, A. M., Wabakanghanzi, J. N., and Six, J.: An initial investigation into the organic matter biogeochemistry of the Congo River. Geochim. Cosmochim. Acta 84, 614-627, doi:10.1016/j.gca.2012.01.013, 2012.

Standing committee of Analysts: Ammonia in waters. Methods for the examination of waters and associated materials. 16 pp., 1981.

Stanley, E. H., Casson, N. J., Christel, S. T., Crawford, J. T., Loken, L. C., Oliver, S. K.: The ecology of methane in streams and rivers: patterns, controls, and global significance. Ecol. Mon., 86, 146-171, doi:10.1890/15-1027, 2016.

Still, C. J., and Powell, R. L.: Continental-scale distributions of vegetation stable carbon isotope ratios. West JB, Bowen GJ, Dawson TE, Tu KP, editors. Isoscapes. Netherlands: Springer Netherlands. p179-193, 2010.

Takahashi, T., Sutherland, S. C., Wanninkhof, R., Sweeney, C., Feely, R. A., Chipman, D. W., Hales, B., Friederich, G., Chavez, F., Sabine, C., Watson, A., Bakker, D. C. E., Schuster, U., Metzl, N., Yoshikawa-Inoue, H.I., Ishii, M., Midorikawa, T., Nojiri, Y., Körtzinger, A., Steinhoff, T., Hoppema, M., Olafsson, J., Arnarson, T. S., Tilbrook, B., Johannessen, T., Olsen, A., Bellerby, R., Wong, C. S., Delille, B., Bates, N. R., de Baar, H. J. W.: Climatological mean and decadal change in surface ocean pCO_2, and net sea-air CO_2 flux over the global oceans, Deep-Sea Res. II, 56, 554-577, doi: 10.1016/j.dsr2.2008.12.009, 2009.

Tamooh, F., Borges, A. V., Meysman, F. J. R., Van Den Meersche, K., Dehairs, F., Merckx, R., and Bouillon, S.:Dynamics of dissolved inorganic carbon and aquatic metabolism in the Tana River basin, Kenya, Biogeosciences, 10, 6911–6928, doi:10.5194/bg-10-6911-2013, 2013

Teodoru, C. R., Nyoni, F. C., Borges, A. V., Darachambeau, F., Nyambe, I., and Bouillon, S.: Spatial variability and temporal dynamics of greenhouse gas (CO_2, CH_4, N_2O) concentrations and fluxes along the Zambezi River mainstem and major tributaries. Biogeosciences, 12, 2431-2453. doi:10.5194/bg-12-2431-2015, 2015.

Tyler, S.C., Bilek, R.S., Sass, R.L., and Fisher, F.M.: Methane oxidation and pathways of production in a Texas paddy field deduced from measurements of

flux, $\delta^{13}C$, and δD of CH_4. Global Biogeochem. Cycles, 11, 323-348, doi: 10.1029/97GB01624, 1997.

Ulseth, A. J., Hall Jr, R. O., Canadell, M. B., Madinger, H. L., Niayifar, A., and Battin, T. J.: Distinct air–water gas exchange regimes in low- and high-energy streams. Nature Geoscience 12, 259-263, doi: 10.1038/s41561-019-0324-8, 2019

Upstill-Goddard, R. C., Salter, M. E., Mann, P.J., Barnes, J., Poulsen, J., Dinga, B., Fiske, G. J., and Holmes, R. M.: The riverine source of CH_4 and N_2O from the Republic of Congo, western Congo Basin. Biogeosciences, 14, 2267-2281. doi:10.5194/bg-14-2267-2017, 2017.

Ward, N. D., Krusche, A. V., Sawakuchi, H. O., Brito, D. C., Cunha, A. C., Sousa Moura, J. M., da Silva, R., Yager, P. L., Keil, R. G., and Richey, J. E.: The compositional evolution of dissolved and particulate organic matter along the lower Amazon River—Óbidos to the ocean. Mar. Chem. 177, 244–256, doi:10.1016/j.marchem.2015.06.013, 2015.

Ward N. D., Sawakuchi, H. O., Neu, V., Less, D. F. S., Valerio, A. M., Cunha , A. C., Kampel, M., Bianchi, T. S., Krusche, A. V., Richey, J. E., Keil, R. G.: Velocity-amplified microbial respiration rates in the lower Amazon River, Limnol. Oceanogr. Lett., 3, 2018, 265–274, doi: 10.1002/lol2.10062, 2018.

Wassenaar, L. I., Coplen, T. B., and Aggarwal, P. K.: Approaches for achieving long-term accuracy and precision of $\delta^{18}O$ and δ^2H for waters analyzed using laser absorption spectrometers, Environ. Sci. Technol., 48, 1123-1131, doi: 10.1021/es403354n, 2014.

Weiss, R. F., Price, B. A.: Nitrous oxide solubility in water and seawater. Mar. Chem. 8, 347-359, doi: 10.1016/0304-4203(80)90024-9, 1980.

Weiss, R.F.: Determinations of carbon dioxide and methane by dual catalyst flame ionization chromatography and nitrous oxide by electron capture chromatography. J. Chromatogr. Sci., 19, 611-616, doi: 10.1093/chromsci/19.12.611, 1981.

Wissmar, R. C., Richey, J. E., Stallard, R. F., and Edmond, J. M.: Plankton metabolism and carbon processes in the Amazon river, its tributaries, and floodplain waters, Peru-Brazil, May-June 1977. Ecology, 62, 1622-1633, doi: 10.2307/1941517, 1981.

Yoshida, N., Iguchi, H., Yurimoto, H., Murakami, A., and Sakai, Y.: Aquatic plant surface as a niche for methanotrophs. Frontiers Microbiol., 30, 1-9, doi:10.3389/fmicb.2014.00030, 2014.

Zhou, L., Tian, Y., Myneni, R. B., Ciais, P., Saatchi, S. L., Yi Y., Shilong, P., Chen, H., Vermote, E. F., Song, C., and Hwang, T.: Widespread decline of Congo rainforest greenness in the past decade, Nature, 509, 86-90, doi:10.1038/nature13265, 2014.

Table 1: Partial pressure of CO_2 (pCO_2 in ppm), dissolved CH_4 concentration (nmol L^{-1}), dissolved N_2O saturation level (%N_2O in %), gas transfer velocity (k_{600} in cm h^{-1}), air-water fluxes of CO_2 (FCO_2 in mmol m^{-2} d^{-1} and in TgC yr^{-1}), of CH_4 (FCH_4 in µmol m^{-2} d^{-1} and in TgCH$_4$ yr^{-1}), of N_2O (FN_2O in µmol m^{-2} d^{-1} and in GgN$_2$O-N yr^{-1}), stream surface area (S.A. in km^2), as a function of Strahler stream order (S.O.) in the Congo River network for rivers and streams draining and not draining the Cuvette Centrale Congolaise.

S.O.	pCO$_2$ ppm	CH$_4$ nmol L^{-1}	N$_2$O nmol L^{-1}	%N$_2$O %	k$_{600}$ cm h^{-1}	Temp. °C	FCO$_2$ mmol m^{-2} d^{-1}	FCH$_4$ µmol m^{-2} d^{-1}	FN$_2$O µmol m^{-2} d^{-1}	S.A. km^2	FCO$_2$ TgC yr^{-1}	FCH$_4$ TgCH$_4$ yr^{-1}	FN$_2$O GgN$_2$O-N yr^{-1}
Draining the Cuvette Centrale Congolaise													
1	12,304	8,349	0.5	7.3	26.4	27.0	2,892	61,732	-43.1	350	4.4	0.126	-0.154
2	12,304	8,349	2.7	44.1	16.1	27.0	1,766	37,747	-15.9	335	2.6	0.074	-0.054
3	11,923	7,411	4.9	77.5	13.0	26.1	1,376	25,765	-5.2	324	2.0	0.049	-0.017
4	12,065	9,409	6.5	104.5	12.3	26.7	1,323	33,431	0.9	291	1.7	0.057	0.003
5	13,705	9,533	2.0	32.2	12.5	27.0	1,525	33,255	-14.8	278	1.9	0.054	-0.042
6	7,830	532	13.2	214.7	12.2	27.5	834	1,855	24.7	480	1.8	0.005	0.121
7	6,643	503	11.3	188.8	11.7	27.5	670	1,582	18.2	163	0.5	0.002	0.030
8	6,977	401	12.9	219.8	13.6	28.7	824	1,581	28.6	366	1.3	0.003	0.107
Not draining the Cuvette Centrale Congolaise													
1	10,719	1,584	9.4	136.6	161.6	24.1	15,417	66,695	107.2	2235	150.9	0.871	2.449
2	8,921	1,275	9.4	135.8	56.5	24.1	4,450	19,171	36.4	2143	41.8	0.240	0.798
3	7,225	1,185	9.3	133.4	31.1	24.0	1,972	9,554	18.9	1883	16.3	0.105	0.364
4	5,766	726	8.5	126.3	21.5	24.3	1,065	4,098	10.1	1752	8.2	0.042	0.181
5	4,110	538	8.6	131.4	17.2	25.5	589	2,452	9.6	1688	4.4	0.024	0.165
6	1,929	299	9.3	143.4	16.8	25.6	239	1,328	12.9	1772	1.9	0.014	0.233
7	2,667	220	9.3	153.6	16.3	27.5	343	1,030	15.4	2168	3.3	0.013	0.340
8	3,010	226	6.7	109.2	12.9	27.7	310	837	2.1	1696	2.3	0.008	0.036
9	2,521	170	8.7	145.7	10.9	27.7	217	533	8.8	4639	4.4	0.014	0.419
10	3,445	33	9.4	153.1	20.4	27.7	574	178	19.2	646	1.6	0.001	0.127
Total													
											251	1.7	5.1

Figure 1: Freshwater discharge (m^3 s^{-1}) of the Congo River at Kinshasa from 2010 to 2015, with an indication of field expedition duration (thick lines).
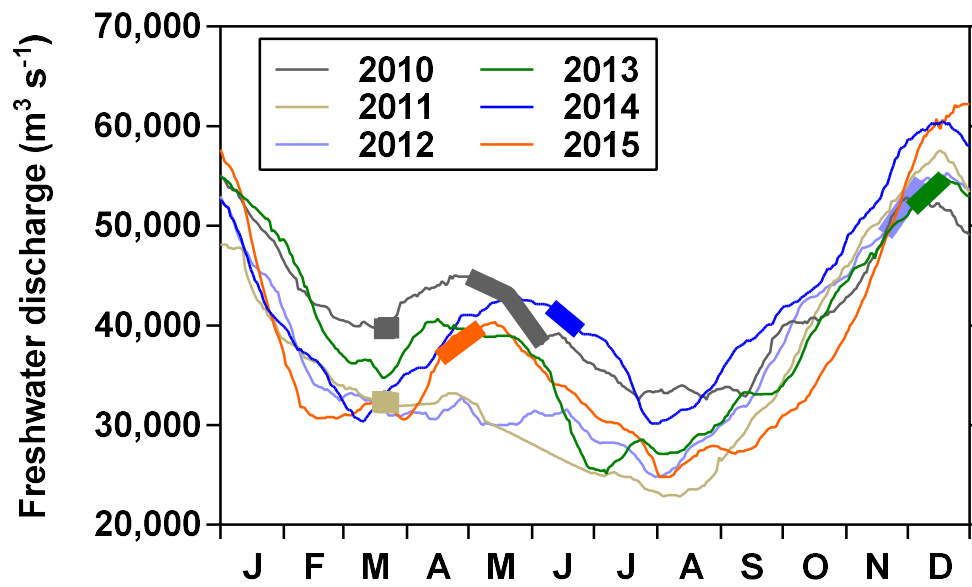
Figure 2: Map showing the sampling stations of the ten field expeditions in the Congo River network.

Figure 3: Variation in surface waters of the specific conductivity (µS cm⁻¹), water temperature (°C), oxygen stable isotope composition of H₂O (δ^{18}O-H₂O in ‰), total suspended matter (TSM in mg L⁻¹), total alkalinity (TA in µmol kg⁻¹), dissolved organic carbon (DOC in mg L⁻¹), carbon stable isotope composition of dissolved inorganic carbon (δ^{13}C-DIC in ‰), pH, partial pressure of CO₂ (pCO₂ in ppm), dissolved O₂ saturation level (%O₂ in %), dissolved CH₄ concentration (nmol L⁻¹), dissolved N₂O saturation level (%N₂O in %) as a function of the distance upstream of Kinshasa along a transect along the Congo River from Kisangani (03/12/2013-19/12/2013, *n*=10,505). Grey and black symbols indicate samples from the mainstem and green samples from tributaries.

Figure 4: Variation in surface waters of the specific conductivity (µS cm^{-1}), water temperature (°C), oxygen stable isotope composition of H$_2$O (δ^{18}O-H$_2$O in ‰), total suspended matter (TSM in mg L^{-1}), total alkalinity (TA in µmol kg^{-1}), dissolved organic carbon (DOC in mg L^{-1}), carbon stable isotope composition of dissolved inorganic carbon (δ^{13}C-DIC in ‰), pH, partial pressure of CO$_2$ (pCO$_2$ in ppm), dissolved O$_2$ saturation level (%O$_2$ in %), dissolved CH$_4$ concentration (nmol L^{-1}), dissolved N$_2$O saturation level (%N$_2$O in %) as a function of the distance upstream of Kinshasa along a transect along the Congo River from Kisangani (10/06/14-30/06/14, n=12,968). Grey and black symbols indicate samples from the mainstem and green samples from tributaries.
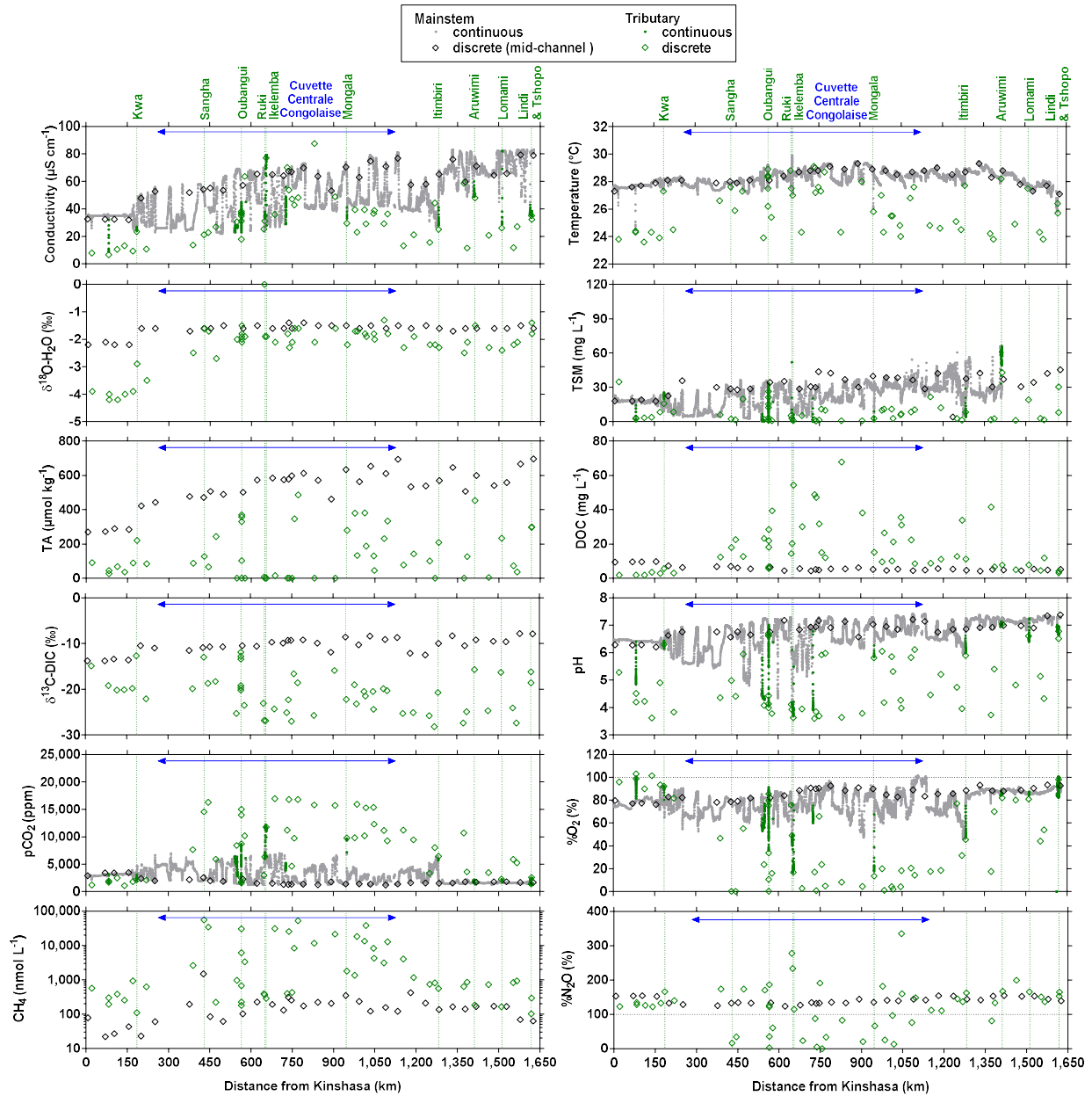
Figure 5: Carbon stable isotope composition of CH_4 ($\delta^{13}C$-CH_4 in ‰) in surface waters of the Congo River mainsteam (black symbols) and tributaries (green symbols) as a function of dissolved CH_4 concentration (nmol L^{-1}) and as function of the distance upstream of Kinshasa, obtained along a longitudinal transect along the Congo River from Kisangani (10/06/14-30/06/14). Dotted line indicates linear regression.
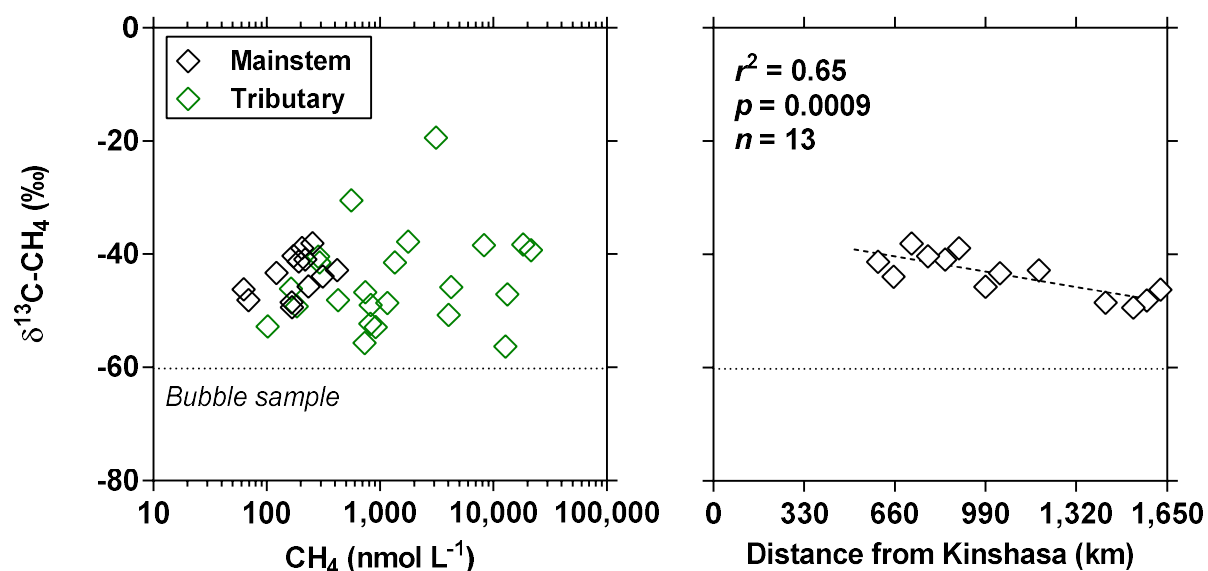
Figure 6: Carbon stable isotope composition of particulate organic carbon (δ^{13}C-POC in ‰) in surface waters of the Congo River network as a function of dissolved O_2 saturation level (%O_2 in %) and dissolved CH_4 concentration (nmol L^{-1}). Grey lines indicate average (full line) and standard deviation (dotted lines) of average soil organic carbon stable isotope composition with a dominance of C_4 (-15.5±0.8 ‰) and C_3 plants (-28.4±0.7 ‰) (Bird and Pousai 1997). Data with δ^{13}C-POC < -30‰ were associated to significantly lower %O_2 and higher CH_4 than data with δ^{13}C-POC > -30‰ (Mann-Whitney *p*<0.0001 for both tests).
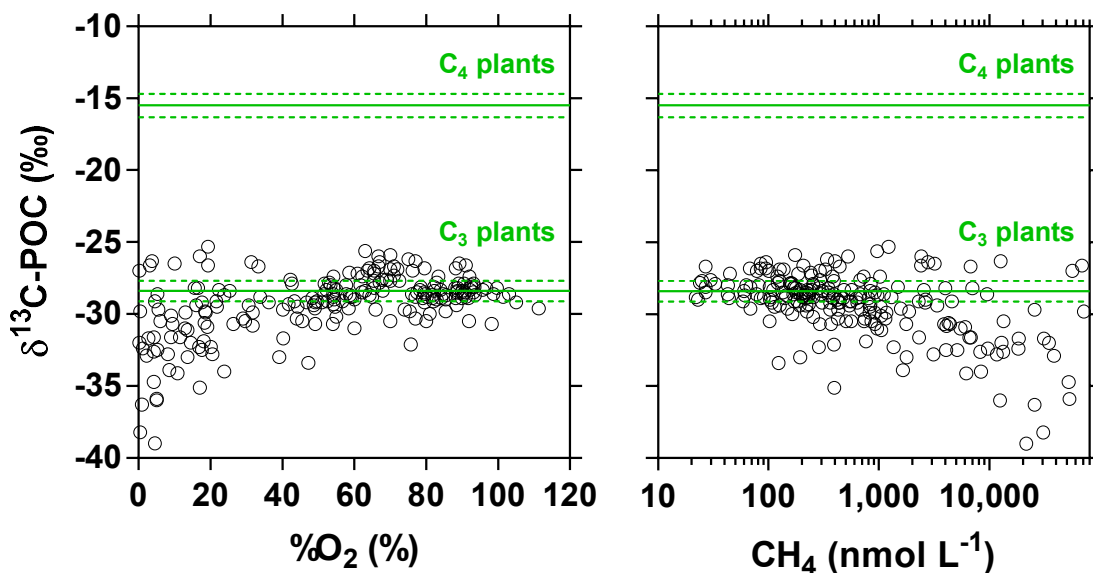
Figure 7: Dissolved N_2O saturation level (%N_2O in %), ratio of NH_4^+ to dissolved inorganic nitrogen (DIN=NH_4^++NO_2^-+NO_3^-) (µmol:µmol), and ratio of NO_3^- to DIN (µmol:µmol) in surface waters of the Congo River network as a function of dissolved O_2 saturation level (%O_2 in %). Outliers (red dots) were identified with a Cook's Distance procedure and removed prior linear regression analysis (solid line).
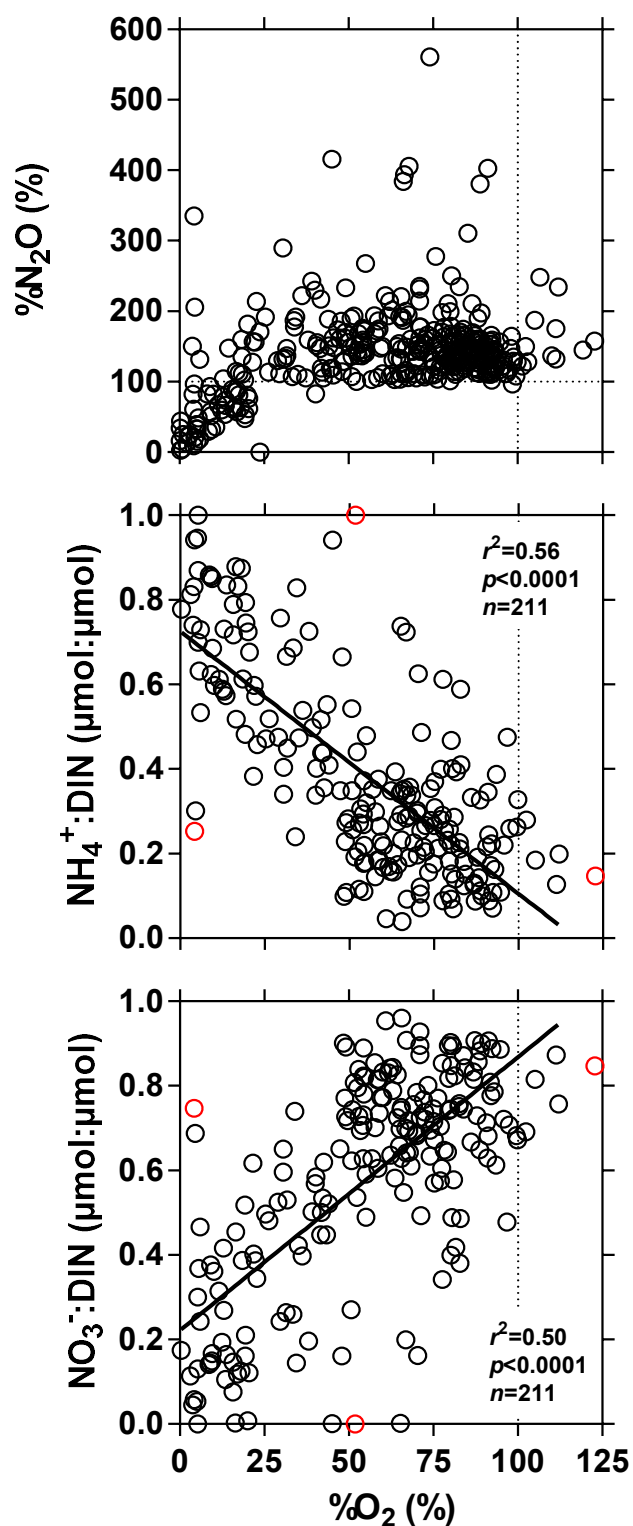
Figure 8: Dissolved N_2O saturation level ($\%N_2O$ in %), as a function of the ratio of NH_4^+ to dissolved inorganic nitrogen ($DIN=NH_4^++NO_2^-+NO_3^-$) (µmol:µmol), and of the ratio of NO_3^- to DIN (µmol:µmol) in surface waters of the Congo River network. Outliers (red dots) were identified with a Cook's Distance procedure and removed prior linear regression analysis (solid line).
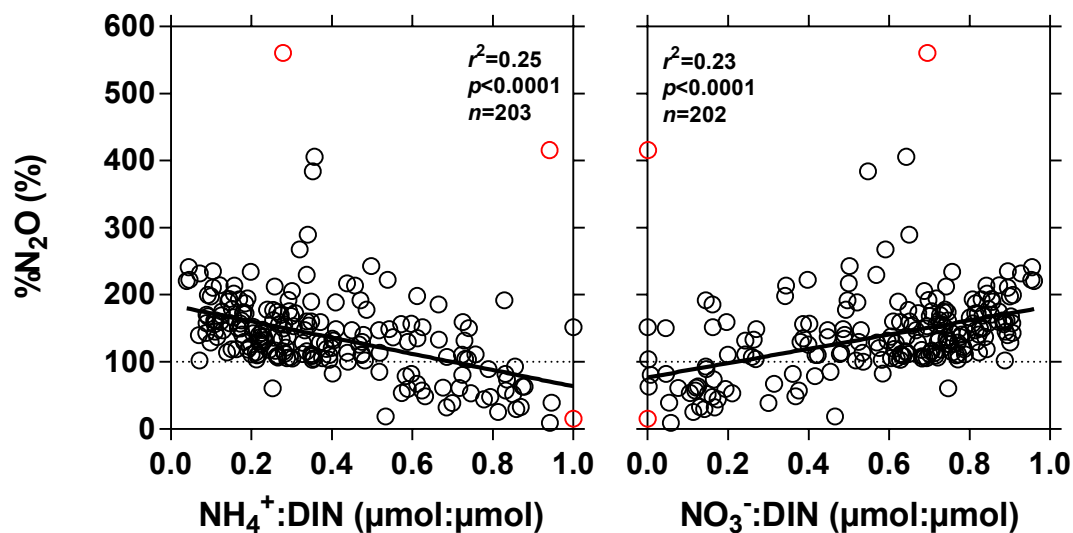
Figure 9: Variations in surface water of the partial pressure of CO_2 (pCO_2 in ppm), dissolved oxygen saturation level (%O_2 in %), pH, specific conductivity ($\mu S\ cm^{-1}$), water temperature (°C) and total suspended matter (TSM in mg L^{-1}) along perpendicular transects to the mainstem Congo River as function of distance from the left bank (m), and at a variable distance from Kinshasa (10/06/14-30/06/14).
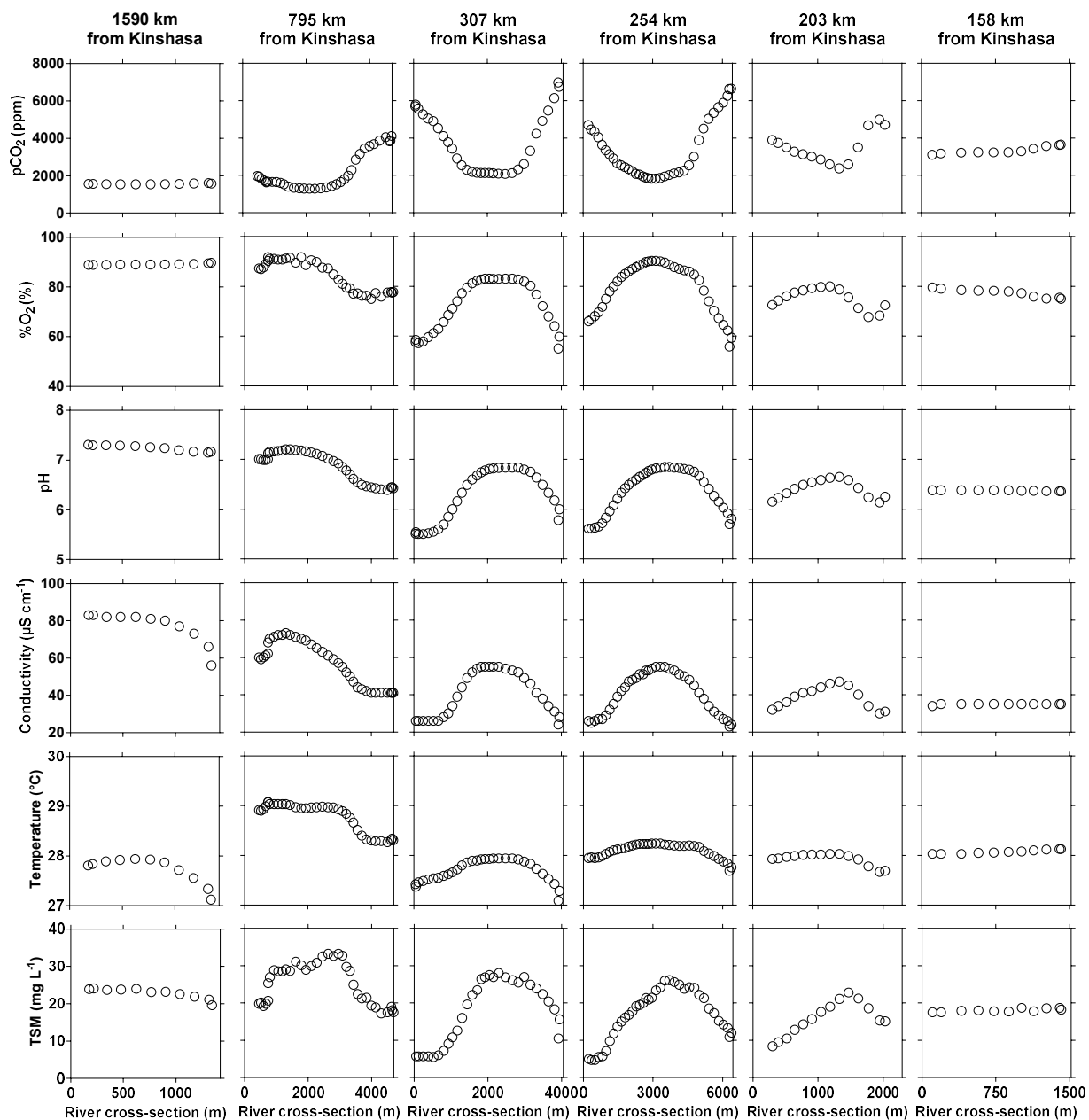
Figure 10: Variation in surface waters of the specific conductivity (µS cm^{-1}), water temperature (°C), oxygen stable isotope composition of H$_2$O (δ^{18}O-H$_2$O in ‰), total suspended matter (TSM in mg L^{-1}), total alkalinity (TA in µmol kg^{-1}), dissolved organic carbon (DOC in mg L^{-1}), carbon stable isotope composition of dissolved inorganic carbon (δ^{13}C-DIC in ‰), pH, partial pressure of CO$_2$ (pCO$_2$ in ppm), dissolved O$_2$ saturation level (%O$_2$ in %), dissolved CH$_4$ concentration (nmol L^{-1}), dissolved N$_2$O saturation level (%N$_2$O in %) as a function of the distance upstream of the Kwa mouth along a transect along the Kwa River (16/04/15-06/05/15, *n*=7,017). Grey and black symbols indicate samples from the mainstem and green samples from tributaries.
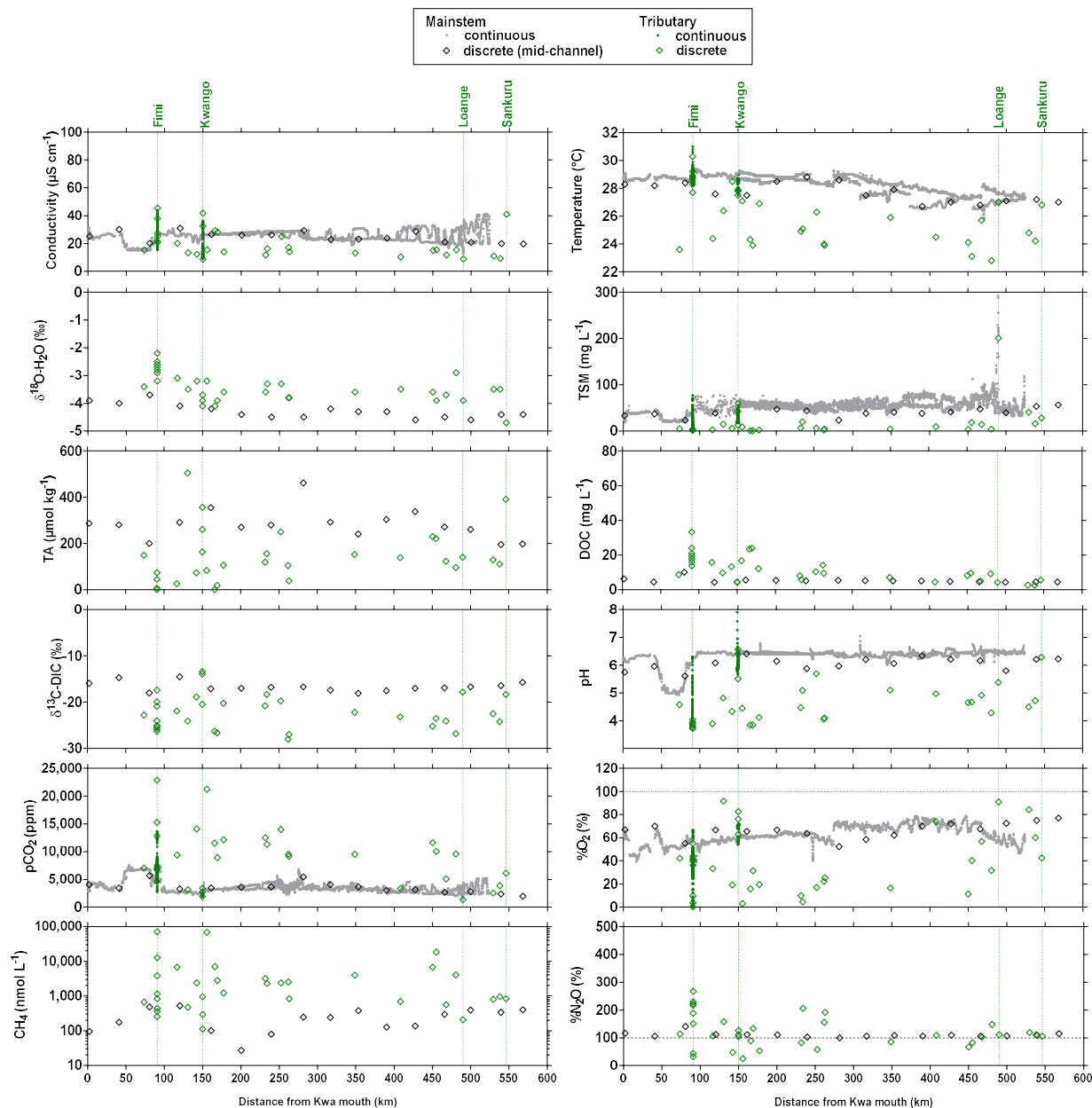
Figure 11: Box plot as function of Strahler stream order of the partial pressure of CO_2 (pCO_2 in ppm), dissolved CH_4 concentration (nmol L^{-1}), dissolved N_2O saturation level (%N_2O in %), and dissolved O_2 saturation level (%O_2 in %) for rivers and streams of the Congo River network draining and not draining the Cuvette Centrale Congolaise. The box represents the first and third quartile, horizontal line corresponds to the median, the cross to the average, error bars correspond to the maximum and minimum, symbols show all data points. A Mann-Whitney test was used to test statistical differences: ns = not significant, **** = p<0.0001; *** = p<0.001; **=p<0.01; *=p<0.05.
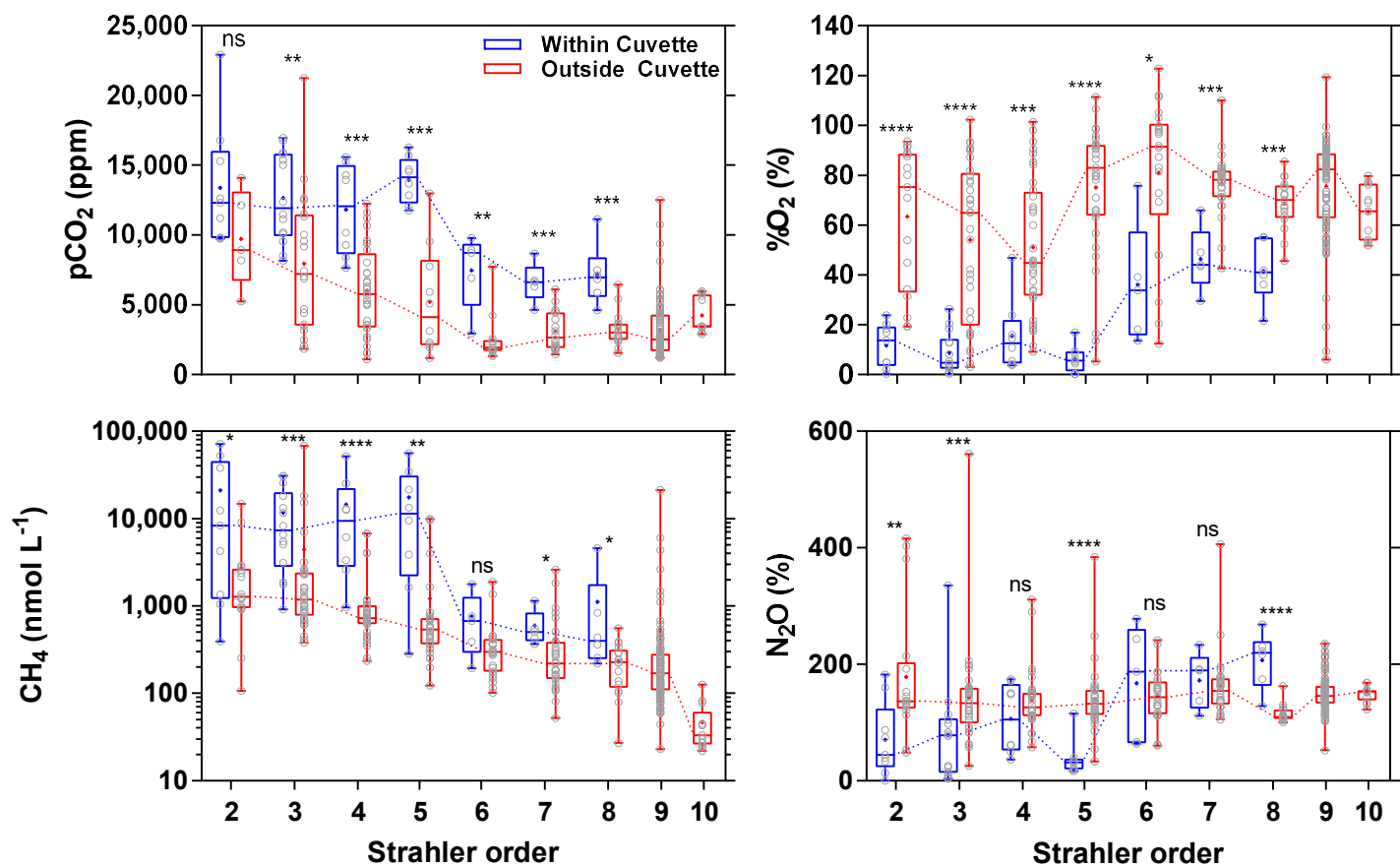
Figure 12: Box plot of the partial pressure of CO_2 (pCO_2 in ppm), dissolved O_2 saturation level (%O_2 in %), dissolved CH_4 concentration (nmol L^{-1}), and dissolved N_2O saturation level (%N_2O in %) in surface waters of rivers and streams of the Congo river network draining and not draining the Cuvette Centrale Congolaise for small and large systems (Strahler stream order 5≤ and >5, respectively) (03/12/2013-19/12/2013; 10/06/14-30/06/14). The box represents the first and third quartile, horizontal line corresponds to the median, the cross to the average, error bars correspond to the maximum and minimum, symbols show all data points. A Mann-Whitney test was used to test statistical differences: **** = p<0.0001; *** = p<0.001; **=p<0.01.
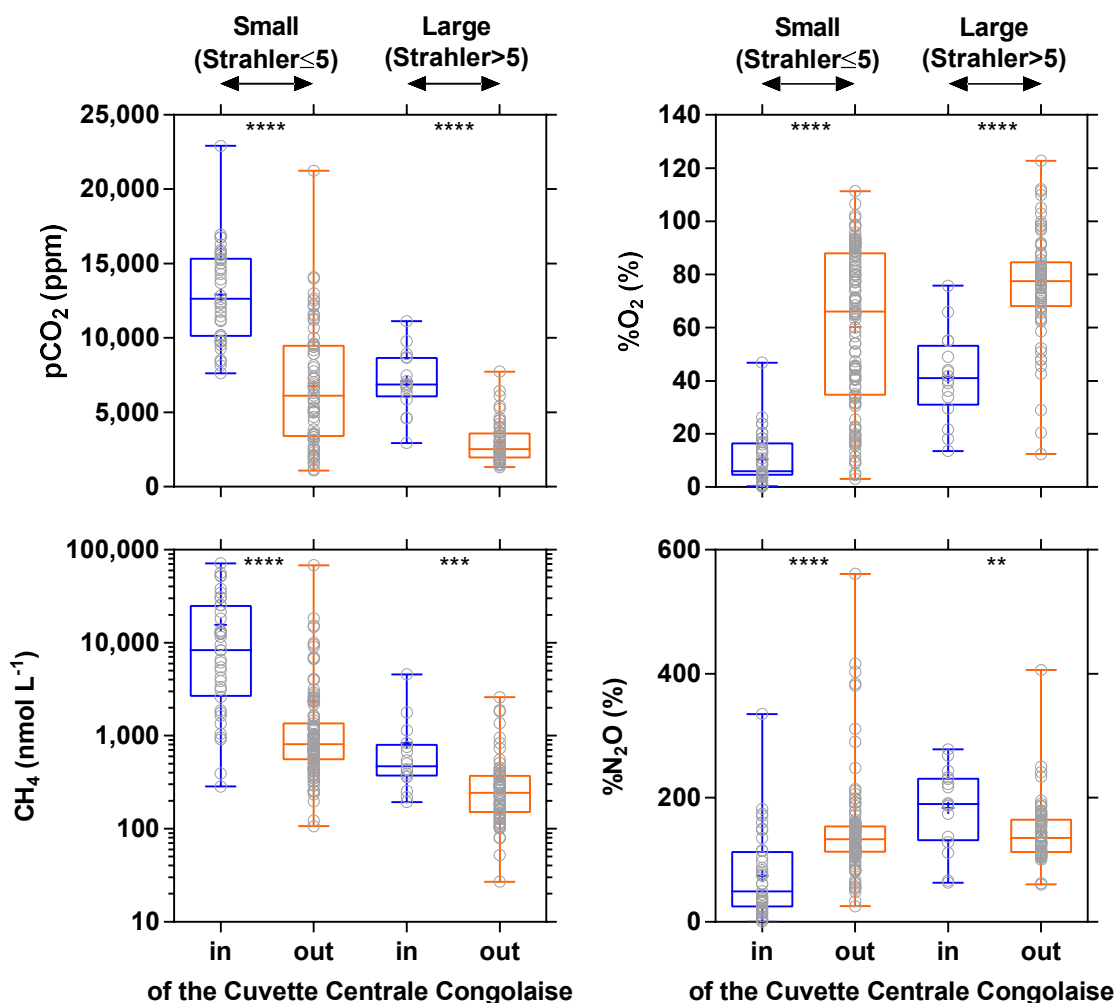
Figure 13: Partial pressure of CO_2 (pCO_2 in ppm) and dissolved O_2 saturation level (%O_2 in %) in surface waters of rivers and streams of the Congo River network as a function of the flooded dense forest over the respective catchment (Global Land Cover 2009). Grey open dots are individual data points, and black full dots are binned averages (± standard deviation) by intervals of 20%.
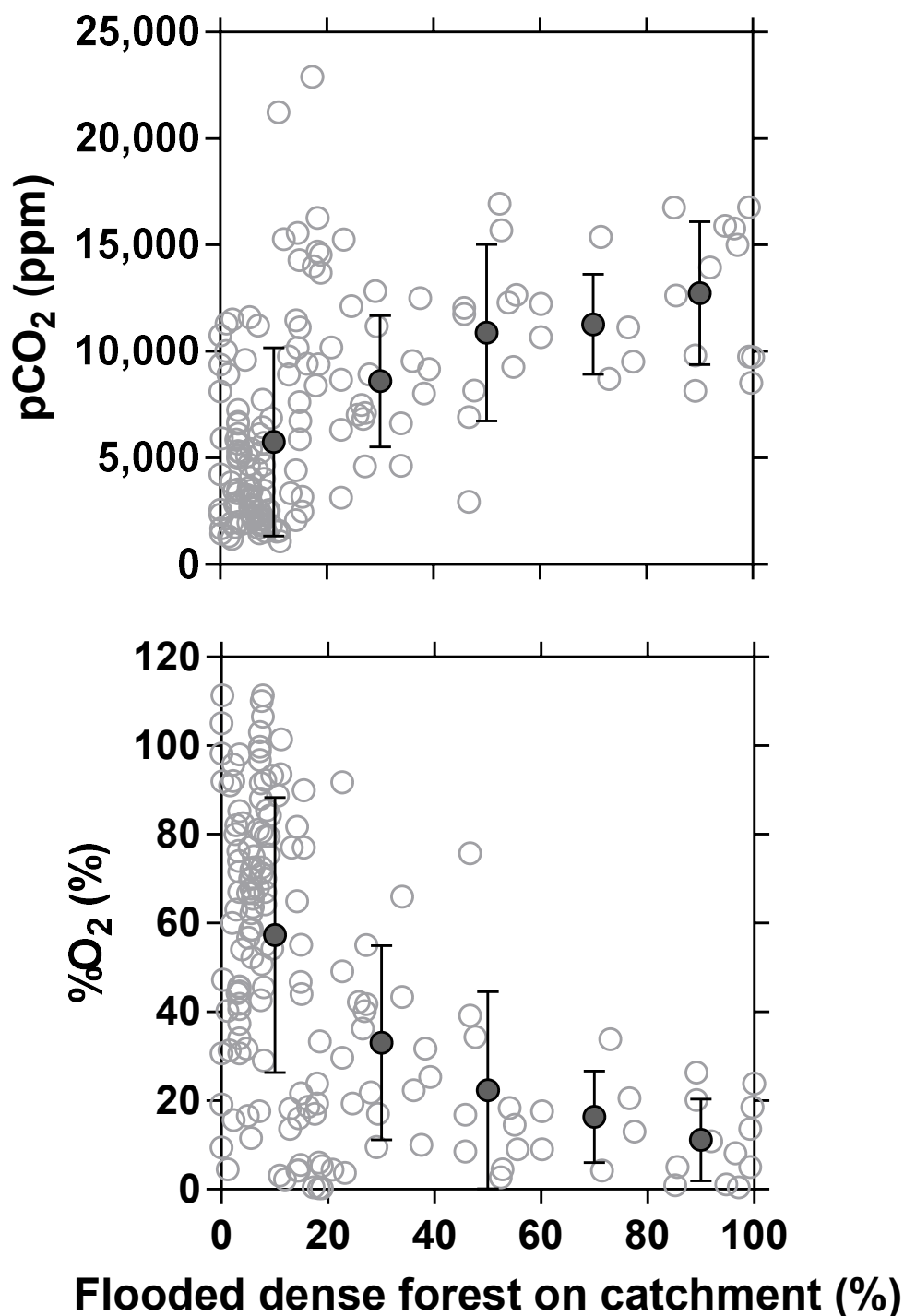
Figure 14: Ratio of dissolved CH_4 and CO_2 concentration (µmol:µmol) plotted as a function of O_2 saturation level (%O_2 in %) and plotted in box plots draining and not draining the Cuvette Centrale Congolaise for small and large systems (Strahler stream order 5≤ and >5, respectively) (03/12/2013-19/12/2013; 10/06/14-30/06/14). The box represents the first and third quartile, horizontal line corresponds to the median, the cross to the average, error bars correspond to the maximum and minimum, symbols show all data points. A Mann-Whitney test was used to test statistical differences: ns=not significant; **** = p<0.0001.
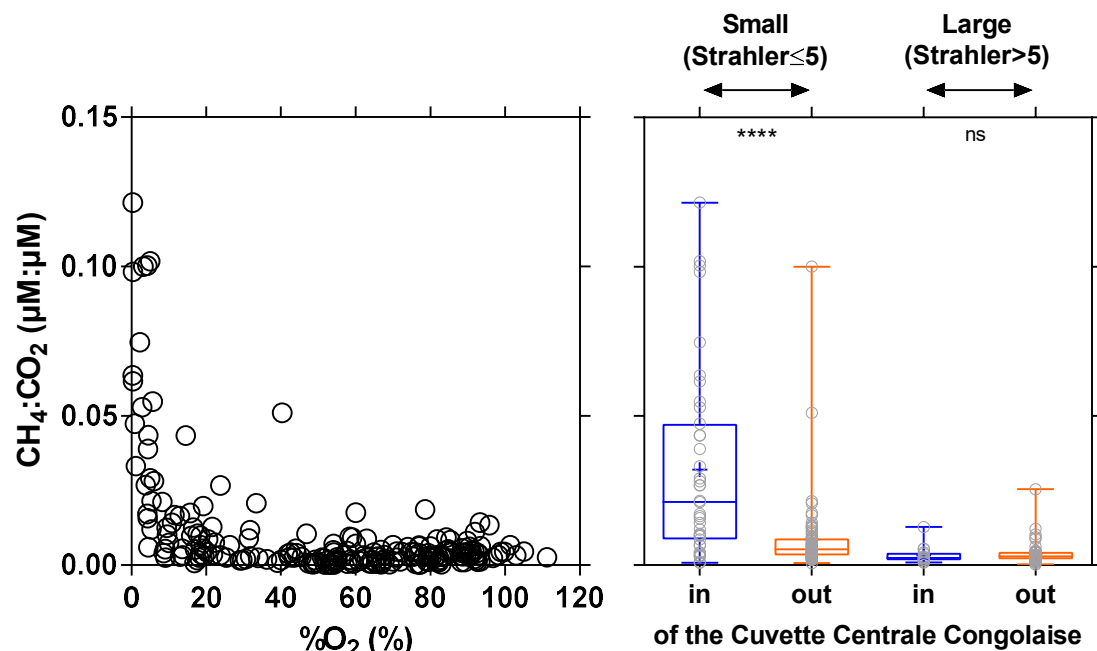
Figure 15: Primary production (measured and modelled) (mmol m^{-2} d^{-1}) as a function of community respiration (mmol m^{-2} d^{-1}), and air-water CO$_2$ fluxes (FCO$_2$ in mmol m^{-2} d^{-1}) as a function of community respiration (mmol m^{-2} d^{-1}) and net community production (mmol m^{-2} d^{-1}) in surface waters of rivers and streams of the Congo River network. Insets show the data in a linear scale (instead of a log-log scale).
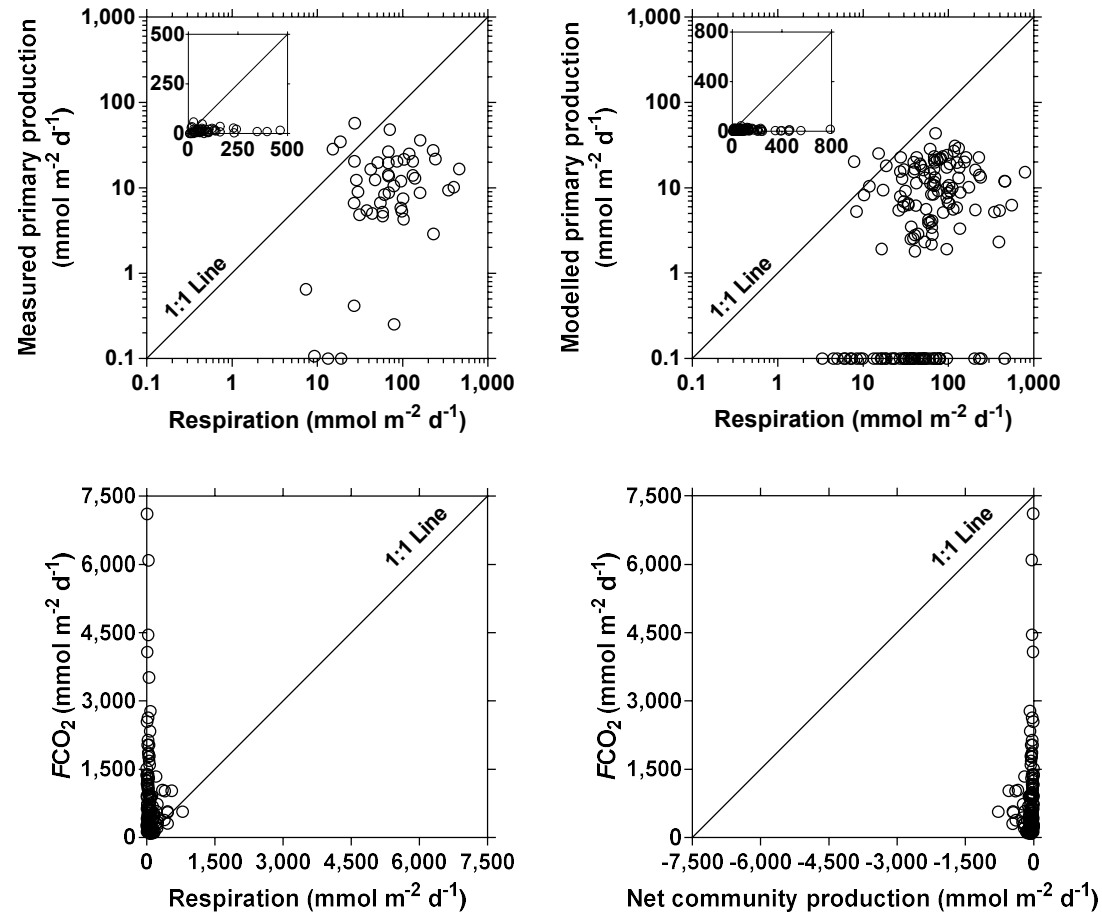
Figure 16: Ratio of air-water CO_2 fluxes (FCO$_2$ in mmol m^{-2} d^{-1}) and community respiration (mmol m^{-2} d^{-1}) as a function of Strahler stream order for rivers and streams of the Congo River network. The box represents the first and third quartile, horizontal line corresponds to the median, the cross to the average, error bars correspond to the maximum and minimum, symbols show all data points. Inset shows in a log scale the median of FCO$_2$:CR and an exponential fit (r^2=0.88).
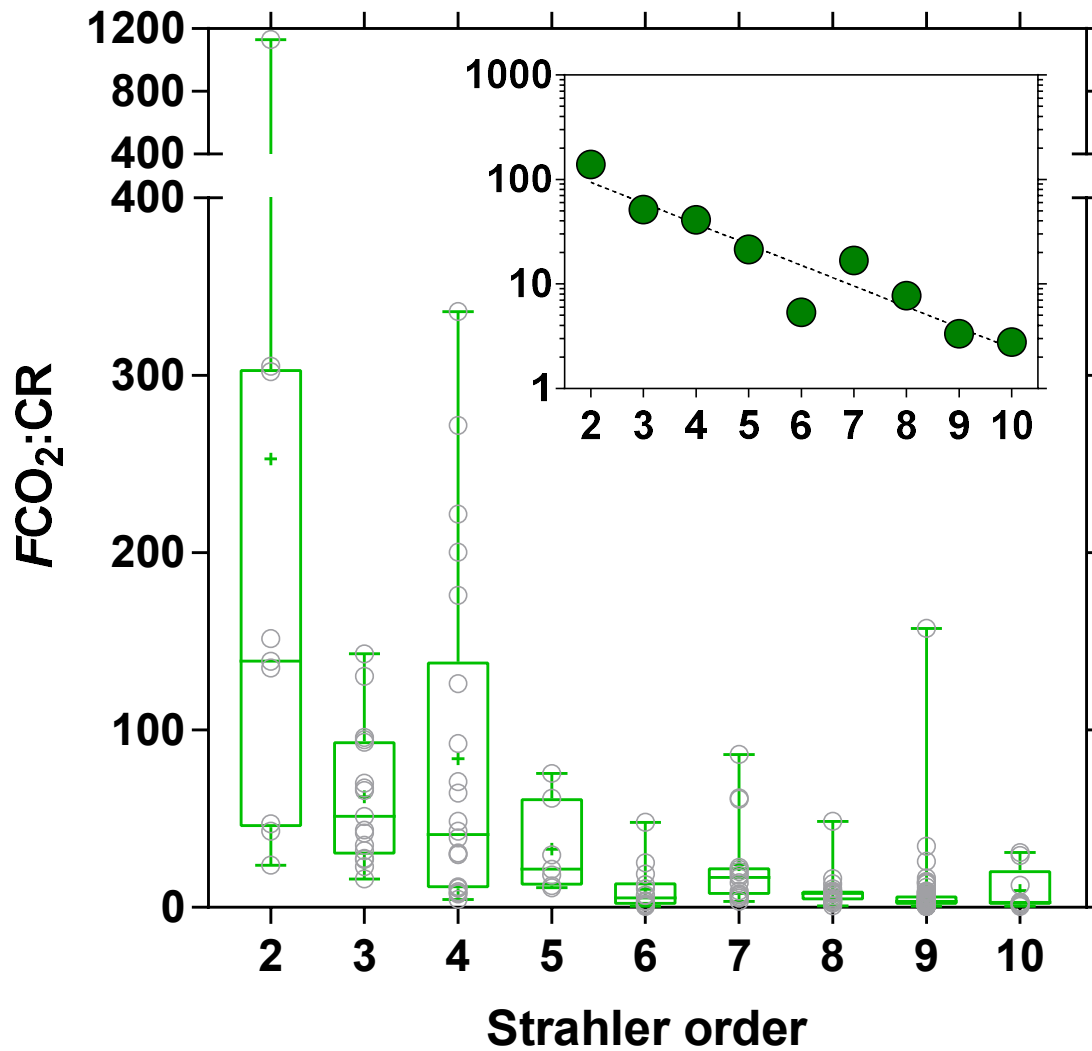
Figure 17: Carbon stable isotope composition of dissolved inorganic carbon (DIC) (δ^{13}C-DIC in ‰) as a function of the total alkalinity (TA) to DIC ratio (µmol:µmol) and as function of the partial pressure of CO_2 (pCO$_2$ in ppm) for a TA:DIC ratio equal to zero in surface waters of of rivers and streams of the Congo River network. Open dots indicate individual data points, full dots indicate binned averages (± stand deviation) (bins <5,000, 5,000-10,000 and >10,000 ppm). Horizontal dotted lines indicate the δ^{13}C values of atmospheric CO_2 and of average soil organic carbon stable isotope composition with a dominance of C$_4$ (-15.5±0.8 ‰) and C$_3$ plants (-28.4±0.7 ‰) (Bird and Pousai 1997). Red dotted line provides polynomial fit (δ^{13}C-DIC = - 22.5 + 21.37 x TA:DIC - 6.97 x TA:DIC, r^2=0.76)
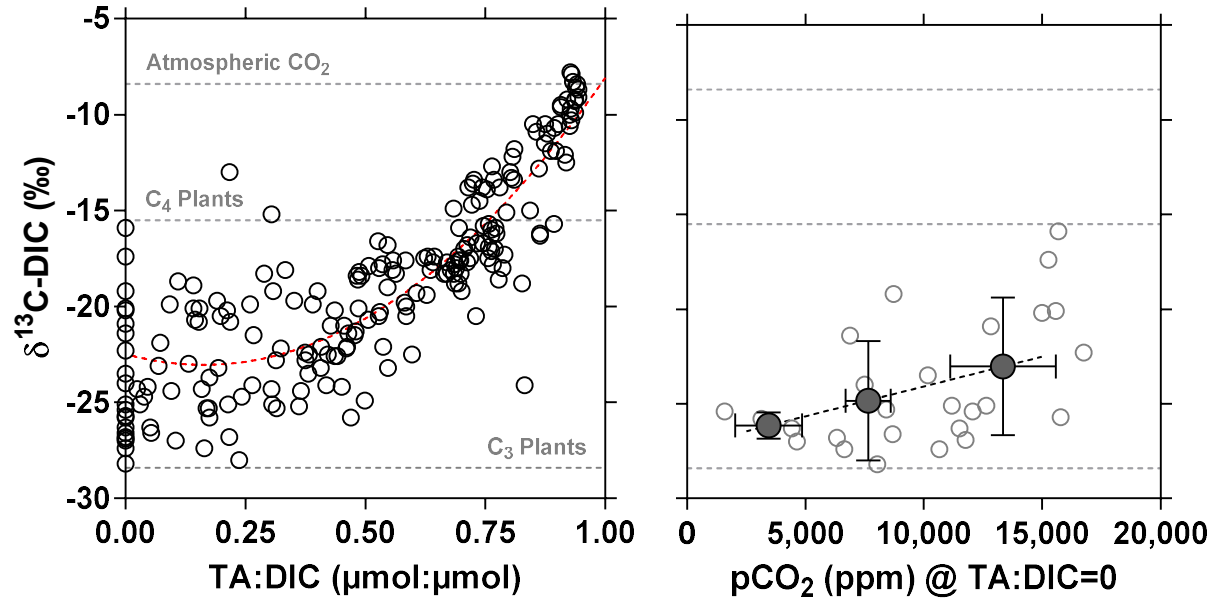
Figure 18: Total alkalinity (TA) and Mg^{2+} as function of Ca^{2+} of the surface waters of rivers and streams of the Congo River network, in Na$^+$ normalized plots (µmol:µmol) showing the composition fields for rivers draining different lithologies from a global compilation of the 60 largest rivers in the World (Gaillardet et al., 1999).
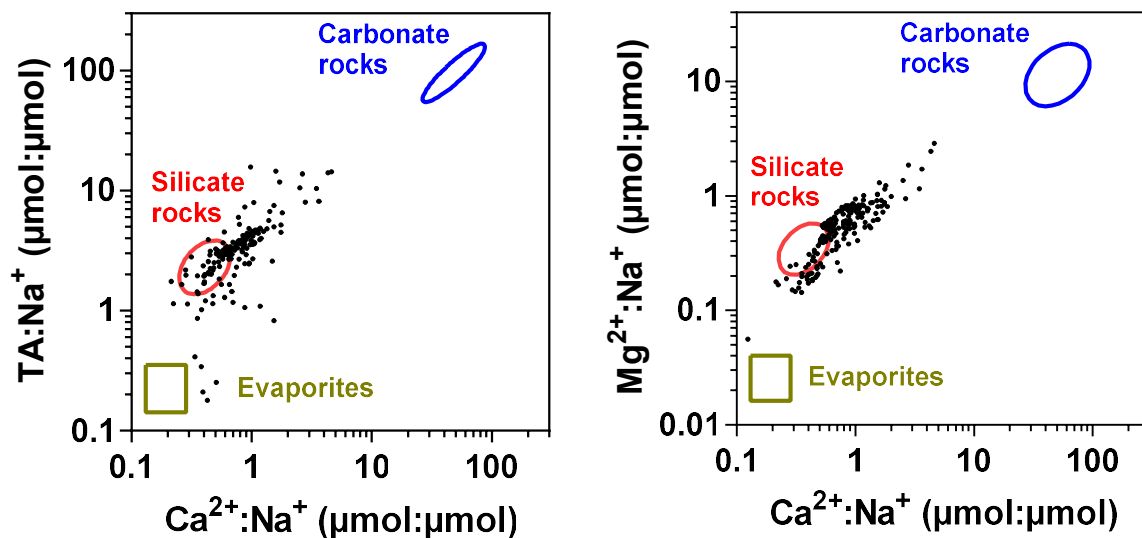
Figure 19: Comparison of the partial pressure of CO_2 (pCO_2 in ppm), dissolved CH_4 concentration (nmol L^{-1}), dissolved O_2 saturation level (%O_2 in %), dissolved N_2O saturation level (%N_2O in %) in surface waters of the Congo River tributaries sampled during both high water (03/12/2013-19/12/2013) and falling water periods (10/06/14-30/06/14). Tributaries were separated into left and right bank, as well as into large and small systems, with a freshwater discharge (Q) < and ≥ 300 m^3 s^{-1}, respectively.
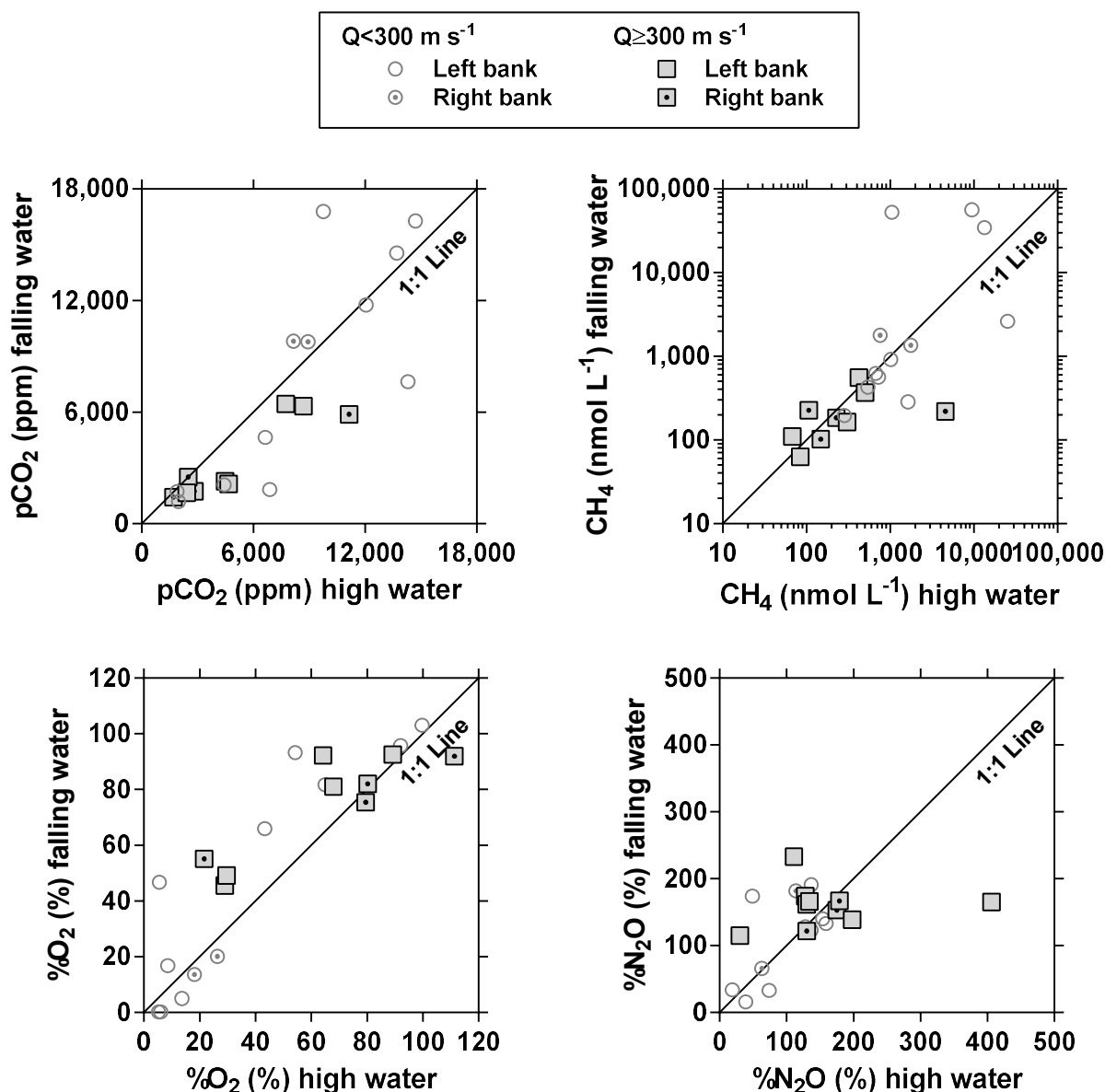
Figure 20: Time series of dissolved CH_4 concentration (nmol L^{-1}) in surface waters and freshwater discharge (grey line) in the Congo River (at Kisangani, 2013-2018), the Oubangui (at Bangui, 2010-2012), and the Kasaï (at Dima, 2015-2017) Rivers. Black line shows a 5 sample running average. Time series of the partial pressure of CO_2 (pCO$_2$ in ppm) in surface waters was also obtained in the Congo River (at Kisangani, 2017-2018). Data in the Oubangui were previously reported by Bouillon et al. (2012; 2013).
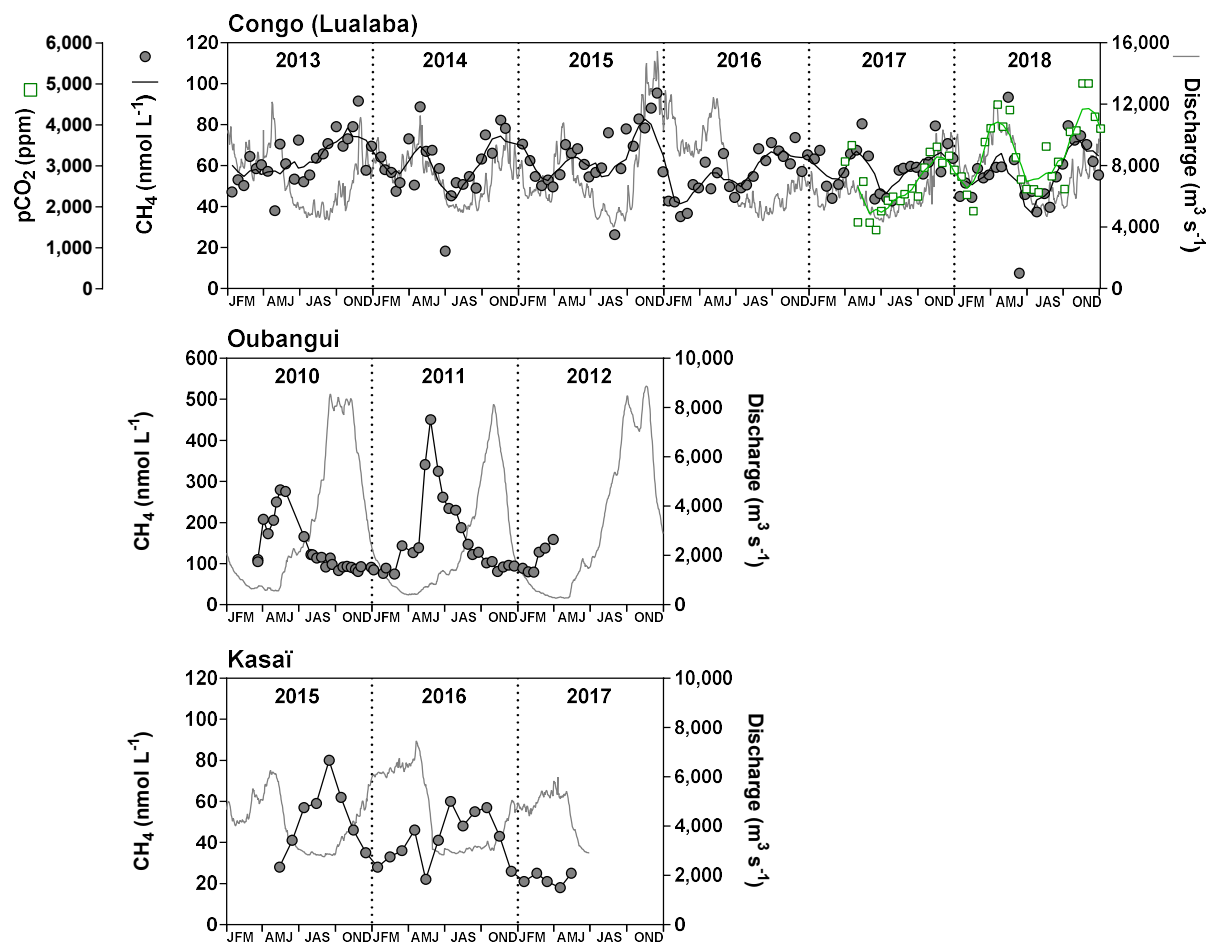
Figure 21: Time series of dissolved N_2O saturation level ($\%N_2O$ in %) in surface waters and freshwater discharge (grey line) in the Congo River (at Kisangani, 2013-2018), the Oubangui (at Bangui, 2010-2012), and the Kasaï (at Dima, 2015-2017) Rivers. Black line shows a 5 sample running average. Data in the Oubangui were previously reported by Bouillon et al. (2012; 2013).
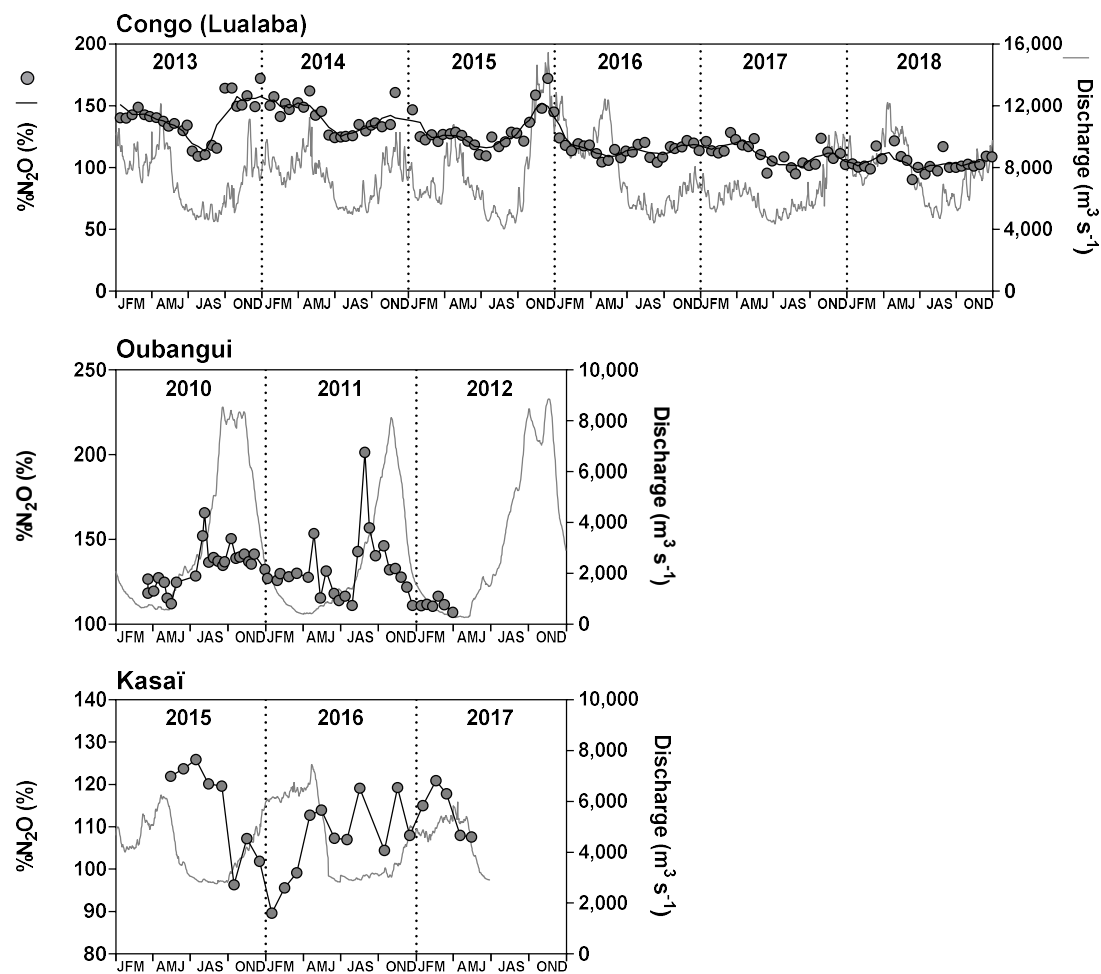
Figure 22: Seasonal amplitude of dissolved CH_4 concentration (ΔCH_4 in nmol L^{-1}) in surface waters as a function of the ratio of seasonal maximum and minimum of freshwater discharge (Qmax:Qmin) in the Congo River (at Kisangani, 2013-2018), the Oubangui (at Bangui, 2010-2012), and the Kasaï (at Dima, 2015-2017) Rivers (Fig. 20).